ON THE CAPACITY OF LARGE-SCALE MIMO SYSTEMS IN SHADOWED FADING CHANNELS

BY

TOLUWANI OLUWATOBI DARAMOLA

A Thesis Presented to the

DEANSHIP OF GRADUATE STUDIES

KING FAHD UNIVERSITY OF PETROLEUM & MINERALS

DHAHRAN, SAUDI ARABIA

In Partial Fulfillment of the
Requirements for the Degree of

MASTER OF SCIENCE

In

TELECOMMUNICATION ENGINEERING

MAY, 2015

KING FAHD UNIVERSITY OF PETROLEUM & MINERALS
DHAHRAN 31261, SAUDI ARABIA

DEANSHIP OF GRADUATE STUDIES

This thesis, written by **TOLUWANI OLUWATOBI DARAMOLA** under the direction of his thesis advisor and approved by his thesis committee, has been presented to and accepted by the Dean of Graduate Studies, in partial fulfillment of the requirements for the degree of **MASTER OF SCIENCE IN TELECOMMUNICATION ENGINEERING**.

Thesis Committee

Dr. Saad Al-Ahmadi (Advisor)

Dr. Azzedine Zerguine (Member)

Dr. Samir Al-Ghadban (Member)

24/5/2015

Dr. Ali Al-Shaikhi
Department Chairman

Dr. Salam A. Zummo
Dean of Graduate Studies

28/5/15

Date

Dedication

To my lovely parents for their prayers and support.

ACKNOWLEDGMENTS

I would like to express my eternal gratitude to the Almighty who gives life and wisdom to be able to complete this thesis work, may we always continue to enjoy His benefits always.

I would like to appreciate ***Dr. Saad M. Al-Ahmadi*** *for his through supervision of this thesis. His support was immense in completing this work. I would like to thank him for his constructive criticisms, his ideas and continuing discussions through the course of my thesis. I appreciate you most sincerely for your trust in my capabilities to be able to handle this work. I appreciate the time you devoted in helping me improve as a researcher.*

My sincere thanks to ***Dr. Azzedine Zerguine*** *for his advice during this thesis work. I highly appreciate the opportunity to benefit from his scientific and research experience. He was always available to help. I also appreciate his advice on writing the thesis and his corrections which helped out a lot.*

Dr. Samir Al-Ghadban *your input to this work is greatly appreciated, thank you for your advice and corrections and for the opportunity to work with and also learn from you.*

A special thanks to The Nigerian Community at KFUPM and my colleagues for their leadership, support, care, advice and companionship.

I would also like to thank ***Dr. Mohamed Deriche*** *and* ***Dr. Saad Al-Abeedi*** *for their leadership, immense support and contribution towards the success of my program. I would like to appreciate* ***Dr. Ali Ahmad Al-Shaikhi*** *for his fatherly care, support and advice at all times.*

My appreciation goes to the ***Saudi Arabian Government*** *through the Ministry of Higher Education for providing the scholarship to be able to enroll for my masters program at KFUPM.*

I owe a lot of thanks to my parents and siblings for their support, patience and love. Thank you for having my back and being there always.

TABLE OF CONTENTS

LIST OF TABLES

LIST OF FIGURES

NOMENCLATURE

Symbol	**Description**
LTE	Long-Term Evolution
LTE-A	Long-Term Evolution Advanced
RF	Radio Frequency
MIMO	Multiple-Input Multiple-Output
SIMO	Single-Input Multiple-Output
MISO	Multiple-Input Single-Output
MU-MIMO	Multi-user MIMO
4G	Fourth generation networks
5G	Fifth generation networks
FDD	Frequency-division duplexing
TDD	Time-division duplexing
IEEE	Institute of Electrical and Electronics Engineers
BS	Base Station
UT	User Terminal
det	Determinant of a Matrix
CSI	Channel State Information
CSIT	Channel State Information at Transmitter

CSIR	Channel State Information at Receiver
SNR	Signal-to-noise ratio
SINR	Signal-to-interference-plus-noise ratio
LOS	Line-of-sight
NLOS	Non-line-of-sight
ZF	Zero-forcing
MRC	Maximal-ratio combining
R.V.	Random Variable
PDF	Probability density function
i.i.d	independent and identically distributed
$\mathcal{CN}$	Circularly-symmetric complex normal
$\mathbb{C}^{M\times M}$	Complex $M \times M$ matrix
$\mathbb{R}^{M\times M}$	Real $M \times M$ matrix
$\mathbf{A}$	Matrix
$\mathbf{a}$	Vector (column-vector)
$\mathbf{a}_i$	Vector indexed for some purpose
a_i	The i.th element of the vector $\mathbf{a}$
a	Scalar
tr ()	Trace of a Matrix
Sec.	Section
Eqn.	Equation

THESIS ABSTRACT

NAME:	TOLUWANI OLUWATOBI DARAMOLA
TITLE OF STUDY:	On the Capacity of Large-Scale MIMO Systems in Shadowed Fading Channels
MAJOR FIELD:	TELECOMMUNICATION ENGINEERING
DATE OF DEGREE:	MAY 2015

Large-scale Multiple-Input and Multiple-Output (MIMO) antenna systems are becoming a viable option for engineers and researchers to improve communication but their performance is affected by both multipath fading and shadowing. This thesis work investigates the achievable rates for the uplink large-scale MIMO under multipath and shadowing conditions. By using maximal ratio combining (MRC) and zero-forcing receivers (ZF) with the assumption of perfect channel state information (CSI), novel expressions for the ergodic capacity using moment-based analysis methods are derived for large-scale MIMO systems under Rician fading for the desired user with Rayleigh and Rician distributed interferers, also novel expressions for the gamma-gamma composite fading model for both independent and fully correlated shadowing at the base station (BS) antenna array are derived.

It is found that as the Rician K-factor increases for the desired user, the capacity increases but the reverse occurs for the interferers. In the case of shadowing, the increase in correlation tends to decrease further the capacity of the desired user. The ZF receiver is found to perform better than the MRC receiver under multipath fading, and also as the number of BS antenna array increases the achievable rate increases with orders of magnitude as comparable with single-antenna BS.

ملخص الرسالة

الاسم الكامل: كلواني الووتوبي دارامولا

عنوان الرسالة: على قدرة أنظمة النطاق الواسع MIMO في القنوات يتلاشى المظللي

التخصص: هندسة الإتصلات

تاريخ الدرجة العلمية: مايو، ٢٠١٥م

أنظمة نطاق واسع المتعددة المدخلات و متعددة المخرجات (MIMO) الهوائيات أصبحت خيارا قابلا للتطبيق للمهندسين وباحثين لتحسين الاتصال ولكن يتأثر أدائها من كل يتلاشى و التظليل المتعددة. هذا العمل الأطروحة يحقق معدلات تحقيقها للوصلة الصاعدة على نطاق واسع MIMO في ظروف تعدد والتظليل. باستخدام القصوى النسبة الجمعي (MRC) و الصفر الإجباري الاستقبالي (ZF) مع افتراض معلومات حالة قناة مثالية (CSI)، و تستمد تعبيرات جديدة للطاقة ارجوديك باستخدام أساليب التحليل القائم على لحظة لأنظمة نطاق واسع MIMO تحت Rician يتلاشى للمستخدم المطلوب بالرايلي (Rayleigh) و Rician التوزيعية وتداخلية، و أيضا تستمد تعبيرات جديدة للنموذج اليتلاشى الغاما–الغاما المركبية لكلا التظليل مستقلة ومترابطة بشكل كامل في المحطة الأساسية (BS) الهوائيات. وجدت أن بزيادات K Rician–عامل للمستخدم المطلوب، يزيد من القدرة ولكن العكس يحدث للتداخل. في حالة التظليل، الزيادة في علاقة تميل إلى مزيد نقصان القدرة المستخدم المطلوب. وجد ان جهاز الاستقبالي ZF، له أداء أفضل من المتلقي MRC تحت اليتلاشى المتعددة، وكذلك كما يزيد عدد من مجموعة BS الهوائي، يزيد أسعار التحقيقي من الزيادات في أوامر من حجم مماثل كما هو الحال مع هوائي واحد BS.

CHAPTER 1

INTRODUCTION

1.1 An Overview of Wireless Communication

Wireless communications has evolved rapidly over the past few decades. We have moved on from the first generation technology which was based on analog systems and made use in Advanced Mobile Phone System (AMPS) deployed in the early 1980's to today's current digital systems based on Long Term Evolution (LTE) that carries voice, data and also Internet Services. It can be said that communication technologies have really evolved, and with this evolution we are able to make efficient use of our smart phones and wireless devices to access the Internet, make group calls while traveling either on a bus, on trains or even in airplanes.

Consequently, there has been an increase in number of users accessing wireless services all over the world and as communication expands from urban to rural areas, the numbers of users increases in a communication network. This in turn causes the network provider to seek better network architecture in order to accommodate

users and also accommodate the increase in data demands on the network.

Engineers and researchers are constantly trying to look at new ways to meet the increasing demand from users for larger bandwidths, higher data rates, faster response times and reliable communications. However wireless communication systems provide a challenge due to bandwidth limitations, power limitations, scarcity of radio frequency (RF) spectrum, channel complexity. Furthermore, there exist a diverse set of channel impairments such as path loss, multipath fading phenomena, scattering, shadowing and interference that makes the communication engineers' task even more difficult.

1.2 Multiple Input Multiple Output (MIMO) systems

In recent research studies [1][2], it has been shown that the Multiple-Input Multiple Output (MIMO) antenna systems is a favorable technology to help tackle the challenges experienced with wireless communication channels. MIMO technology utilizes multiple antennas at both the source which is called the transmitter and the destination which is called the receiver. In MIMO channels received signals are sampled in the spatial domain [1] and then combined in such a way to minimize errors and maximize data throughput by creating constructive multiple parallel data streams. This results in an increase in the throughput and diversity gain which improves overall communication quality. By using MIMO systems, the

multi-path phenomenon can be converted into benefit for wireless communication systems [1][3]. It can also use the benefit of delay spread with random fading to increase transmission rates [4].

MIMO systems have been implemented in different ways and this depends on the use either to combat diversity or increase capacity [5][6]. It also offers many benefits like beam forming gain, spatial diversity and spatial multiplexing [6]. When using multiple antennas it is possible to utilize other benefits rather than array gains and diversity [1], by increasing the data transfer rate using the spatial multiplexing ability of MIMO channels. Commercially MIMO systems have now become a standard for current cellular systems,e.g. IEEE 802.16e and IEEE 802.11 wireless standards. MIMO technology can be implemented by utilizing different approaches viz by space- time coding, antenna selection, and beamforming [1].

Currently the standards in wireless which includes both IEEE 802.11n/11ac (WiFi) and 3GPPLTE-A have adopted MIMO techniques to achieve an increase in spectral efficiency and also reliability. However these standards only access some of the potential benefits of MIMO systems, because they use only a small number of antennas(about 2-8) and achieve efficiencies of only about 15 bps/Hz or less [7]. The need for higher data rates has motivated the need for larger number of antennas. Large-scale MIMO system has become a candidate to support higher data rate demands in 5G (Fifth generation) networks [8][9] and future communication systems. Large-scale MIMO systems equipped with tens to hundreds of antennas

are capable of multigigabit rate transmissions at high spectral efficiencies of the order of tens to hundreds of bps/Hz.

Large-scale MIMO systems have become an area of interest in wireless communications. Researchers at Lunds University and National Instruments recently prototyped a scalable 128-antenna MIMO testbed for 5G wireless research which is capable of real-time, two-way communication over frequency bands and also offers the ability to accommodate more users at higher data rates with better reliability while consuming less power and promises significant gains [10]. In the developed prototype the base station uses a system design factor of 10 base station antenna elements per user terminal (UT), providing 10 users with simultaneous, full bandwidth access to the 100 antenna base station. The large-scale MIMO application framework supports up to 20 MHz of instantaneous real-time bandwidth that scales from 64 to 128 antennas and can be used with multiple independent UTs [10].

Marzetta in his research in [11] showed that under realistic propagation conditions large-scale MIMO can achieve a transmission rate of 17Mb/s for about 40 users in a 20MHz channel in either uplink and downlink directions, producing an average data rate of 730Mb/s per cell and an overall spectral efficiency of 26.5 bits/s/Hz.

1.3 Thesis Scope and Motivation

In conventional MIMO systems, the antenna array is limited to a few antennas, but with large-scale MIMO systems the antenna arrays can comprise up to a hundred or few hundreds of antennas. Though higher rates can be achieved with an increase in antennas but the analysis of large-scale MIMO systems differs from conventional MIMO systems because things that initially start as random become deterministic due to the presence of large arrays [12].

Inter-user interference still persists in the setup of large-scale MIMO systems, complex techniques can be used to mitigate interference and improve performance. As the size of the antenna arrays increases, the impacts of small scale fading cancels out but large-scale fading still persists due to the presence of large array of antennas. With the implementation of a large array at the BS, the random channel vectors between users and the BS become pairwise orthogonal [12], based on literature review, there are several problems that are still open on large-scale MIMO systems and considered to be the motivation of this thesis.

The main aim of this thesis is to provide moment based analysis for the performance of large-scale MIMO capacity when subjected to both multipath and shadowing conditions. The analysis is based on Uplink (transmission from users to BS) large-scale MIMO with perfect Channel State Information (CSI) and using maximal ratio combining (MRC) and zero forcing (ZF) receivers for the analysis.

1.4 Thesis Contributions

In this thesis, using moment-based analysis, new bounds for the ergodic capacity of large-scale MIMO when subjected to multipath and shadowing conditions is derived. For the first part of the derivations the large scale fading due to shadowing is assumed to be held constant. Under this assumption, the large-scale MIMO uplink undergoes Rician fading with Rayleigh interference (Rician/Rayleigh) and also Rician fading with Rician interference (Rician/Rician).

The large-scale MIMO uplink is analyzed with different values of the Rice factor, and the ergodic capacity is derived with different receivers under perfect Channel State Information. The second part of the thesis deals with the case when the shadowing component is random variable. New expressions are derived for large-scale MIMO for both independent shadowing and fully correlated shadowing. New capacity bounds are also derived for these conditions. Monte-Carlo simulations are carried out to verify the new bounds.

1.5 Structure of Thesis

The thesis is categorized into five chapters as follows:

Chapter 1 presents a brief background on the topic considered, the objectives of the thesis and states the contributions of the thesis.

Chapter 2 gives an overview on conventional MIMO, basic terminologies and principles of conventional MIMO systems, with a brief information on large-scale

MIMO systems as a candidate in 5G communications, detection in MIMO systems and also the relevant previously published works .

Chapter 3 deals with multipath fading and derivation of new ergodic capacity bounds using moment based analysis for large-scale MIMO, with large scale shadowing parameter held constant using MRC and ZF receivers (detectors). The effect of interference on capacity in multipath fading is also evaluated.

Chapter 4 deals with large scale shadowing. In this case the shadowing parameter is a random variable with a lognormal distribution. The Gamma-gamma composite fading model is used to derive the ergodic capacity for both independent and correlated cases of shadowing.

Chapter 5 concludes the thesis and proposes future work in the large-scale MIMO area.

CHAPTER 2

BACKGROUND AND LITERATURE REVIEW

2.1 Background

This section gives a brief description of conventional MIMO systems and working principles. It also highlights the relevance of large-scale MIMO systems in current telecommunication networks.

2.1.1 Conventional MIMO Systems

In conventional MIMO wireless channels both the transmitter and the receiver are equipped with N_T and N_R array of antennas respectively, as the number of transmit and receive antennas are increased, the degrees of freedom increases in the propagation channel which leads to an improvement in data rate (high spectral efficiency increase) without necessarily increasing the bandwidth [7], high speed

wireless backhaul connectivity sometimes adopt this type of MIMO configurations. The reliability of this type of MIMO configuration scales according to the link outage probability, on a rapidly varying channel as a function of both time and frequency and where circumstances permit coding across many channel coherence intervals, the achievable rate scales as $\min(N_T,N_R)\log(1+\text{SNR})$, where SNR is the Signal-to-noise ratio [13].

2.1.2 Channel State Information

Having a knowledge about the state of the instantaneous MIMO channel is essential for researchers when designing MIMO systems [6][14]. The knowledge available about the channel is the known as the channel state information (**CSI**). The implementation of the system depends on the information about the knowledge of the channel known by both transmitter and receiver. The receiver[1] is presumed to trace fully the channel fluctuations, but at the transmitter channel acquisition can be quite challenging, this depends on the mechanism employed to split transmission from location X to location Y and also the inversed direction transmission from location Y to point X [15][16]. When the CSI is amended constantly at the transmitter it is aware of the current realization (instantaneous value) of the channel, but in the case when the transmitter is not informed regularly, but it acquires the statistics of the channel (i.e the distribution, the mean

[1]In wireless systems, the user in the downlink scenario for FDD schemes does not usually have the CSI, while at the base stations, the transmitter has access to the CSI easily.

and variance e.t.c).

CSI at the Transmitter ($CSIT$) is where the transmitter has information about the channel gains, and CSI at Receiver ($CSIR$) is where the receiver also has information about the channel gain, for fast fading channels accuracy of channel estimation is a challenge, since the channel varies rapidly, in that case a non-coherent or blind technique is used, and also obtaining CSIT through a feedback system is ineffective in fast fading, but in slow fading channels there is a possibility to approximate the channel gains correctly using pilot assisted transmission [7][11], CSIT based on measured CSI feedback received is effective in such type of channels.

Channel gains is either independent or correlated, and it depends on different factors which include spacing of antenna elements, scattering environments, interferers etc. In some cases the system has limited (statistical) information of the channel at transmitter, Channel Distribution Information at the transmitter (CDIT) is used to update the transmitter about the channel distribution and sometimes the receiver or transmitter may have only the mean or the variance of the channel.

2.1.3 Capacity of MIMO Channels

A very important metric of characterizing any communication channel is known as the ***Channel Capacity***, it serves as a performance measure for communication systems. Capacity is the maximum error-free data rate a channel can support

or the rate per unit bandwidth that can be sustained reliably over the MIMO link [14][17][18]. To ascertain the capacity of the MIMO channel, the common knowledge (mutual information) linking both the transmitted signal vector with the received vector is calculated, signal vector that maximizes the mutual information is determined, MIMO channel capacity depends heavily on the statistical and antenna element correlations of the channel [14].

When transmission rate is greater than capacity the receiving antenna would make decoding inaccuracy with significant likelihood. In MIMO systems capacity is a key factor in such communication links and serves as guide in practical systems for proper design of transmission of signals and processing of received signals.

2.2 Large-scale MIMO and 5G Networks

As 4G (Fourth generation) technologies (LTE and LTE-A) are been deployed over the world, there still an increase in demand from users who have subscriptions to mobile broadband systems every year. Subscribers crave for faster Internet services on the move and with the increase in powerful gadgets and smart phones, users have demanded for increased access speed to be able to cater for advanced media and multimedia capabilities of such devices i.e., video streaming, high-definition voice calls e.t.c. This demand has caused an explosion in wireless mobility and devices, according to European Mobile Observatory there has been about a 92% growth in mobile broadband per year since 2006 [19] and as the number of wireless devices the ability to cater for future capacity challenges has

resulted in the need to explore more research options in 5G networks.

Large-Scale MIMO systems plays a very important role in the setup of 5G networks, it is estimated that the 5G networks has the ability to achieve the capacity of current 4G networks about a 1000 times what is currently on offer [20], the aim of 5G networks is to connect the entire globe with error-free and ever-present communication systems between people to people , machines to machines, people to machines and vice-versa. 5G networks would be able to support communications for higher mobility users like high-speed train users which run on velocities close to 500 km/h. The whole aim of large-scale MIMO systems in 5G will be used to exploit potentially large capacity gains that arises from the use of larger antenna arrays, BS are equipped with large antenna arrays distributed around the cell and are connected via optical fibers to the BS, mobile users have limited number of antennas but together with the BS antenna arrays construct virtual large-scale MIMO links. This technology is currently been deployed and it provides a very interesting area of research [21][22].

2.3 Path loss and Fading

Using wireless radio channels for high-speed communication may sometimes not be highly reliable due to severe challenges poised by susceptibility to noise, interferences, path-loss, shadowing, multi-path and other channel impairments. As the user movements varies all the time, these impairments also change over time due to the mobility of the user. The received signal of the user will vary over time

due to this [23][24].

2.3.1 Path loss, Small-scale Fading and Large-scale Fading

One major cause of fluctuation in the received signal power of users over distances is caused by path-loss. ***Path-loss*** occurs due to power dissipation emitted by the transmitter and the strength of the spreading of channel transmission. An assumption is that the path-loss is always at a given transmit-receive distance [23]. When obstacles are in the transmission path between the transmitter and the receiver, this causes an effect on transmission which is known as ***Shadowing***, this effect attenuates signal power at the receiver through scattering, reflection, diffraction and absorption of signals, if the signal attenuation becomes very strong, the signal at the receiver is blocked.

Multi-path is also an effect that occurs when the signals from the transmitter reaches the receiver by various routes, it is caused by reflection and refraction due to the vicinity of the receiver [23][24]. The magnitude of signal arriving at various paths at the receiver is said to follow a statistical distribution known as *Rayleigh* distribution, this is known as *Rayleigh* fading, but when one component dominates such as a line-of-sight (LOS) component it follows a *Rician* distribution, this is known as *Rician* fading. **Small-Scale Fading** is described by rapid and deep amplitude variations which happens when the user's receiver shifts over distances of a few wavelengths (short travel distances). The fades occur due to multiple reflections (multi-path) owing to surroundings in the vicinity of the receiver. In

narrowband signals, this causes a Rayleigh fading distribution of signal intensity over short distances [25].

Large-Scale fading is caused by shadowing (shadowing variations happens over distances that is correlative to the length of the obstructing body) due to variations in both the profile of the terrain and the nature of the surroundings, and also caused by large scatterers. In deeply shadowed conditions, the received signal strength in the receiver can drop well below that of free space [25][23].

2.3.2 Slow and Fast Fading

In ***Slow*** fading channels, the channels stays almost constant over the entire time while communication occurs where the channel coherence time T_c is far greater than the transmitted symbol period [25]. When the capacity is less than the information rate of transmission, then no detector can recover transmitted codewords from the transmitter and the channel is said to be in *outage* [7][26]. The largest rate of reliable communication when the channel is very poor at a certain outage probability is called the *outage* capacity of the channel. For ***Fast*** fading channels, the channel varies significantly over the entire transmission time, outage does not occur in this channels rather an averaging is done over the time variation of this channel. It is possible to achieve error-free reliable communication for this channel which is known as the *ergodic* capacity [27].

2.3.3 Fading Models

In literature there is a number of distribution models for fading and shadowing, the following are the most commonly used distributions in communication in multipath fading namely :

1. **Rayleigh Distribution**: If X and Y represent two independent and identically distributed (i.i.d.) Gaussian random variables (R.V.) with zero-mean and equal variance σ^2, the envelope $Z = X + \mathrm{j}\,Y$ is Rayleigh-distributed R.V., applying this in wireless communications to the in-phase and quadrature components of a received signal $r(\mathrm{t})$, the signal envelope

$$z(t) = |r(t)| = \sqrt{r_I^2(t) + r_Q^2(t)}, \tag{2.1}$$

has a Rayleigh distribution and its stationary probability density function (PDF) is stated as [28]

$$f_Z(z) = \begin{cases} \frac{z}{\sigma^2}\exp\left(-z^2/2\sigma^2\right) & , \ z \geq 0 \\ 0 & \text{otherwise.} \end{cases} \tag{2.2}$$

2. **Rician Distribution**: When the communication channel has a fixed LOS component then the in-phase and quadrature components are non zero-mean (the variances are equal but different means), and the signal received is the superposition of a LOS component and a complex Gaussian component. The received signal envelope has a Rician distribution [23] and its probability

density is

$$f_Z(z) = \begin{cases} \frac{z}{\sigma^2} I_0\left(\frac{zs}{\sigma^2}\right) \exp\left(\frac{-(z^2+s^2)}{2\sigma^2}\right) & , \ z \geq 0 \\ 0 & \text{otherwise,} \end{cases} \tag{2.3}$$

where $2\sigma^2$ is the mean power in the NLOS multipath components and s^2 is the power of the LOS component, I_0 is the modified Bessel function of the zeroth order [29].

The Rician distribution is some described by a fading parameter K_r which is known as the *Rice factor* and defined as

$$K_r = \frac{s^2}{2\sigma^2}, \tag{2.4}$$

where K_r is a ratio of the power in the LOS components to the power in other (NLOS) multipath components. When $K_r = 0$ the Rician fading becomes Rayleigh and when $K_r = \infty$ there is no fading, therefore the fading parameter K_r serves as to measure the severity of fading, with large K_r it implies mild fading and with small K_r implies severe fading.

3. **Nakagami-m Distribution**: This distribution provides a greater flexibility to model random fading channels better when compared to either Rayleigh or Rician distributions, the parameters of Nakagami-m can be varied to fit

various empirical measurements and is stated as

$$f_Z(z) = \frac{2m^m z^{2m-1}}{\Gamma(m)\Omega^m}\exp\left(\frac{-mz^2}{\Omega}\right) \qquad z \geq 0, \tag{2.5}$$

where Ω is the average received power and $\Gamma(\cdot)$ is the gamma function and m is the fading severity parameter.

When $m = 1$ the distribution in Eqn.(2.5) reduces to the Rayleigh fading and with $m = (K_r+1)^2/(2K_r+1)$ the distribution approximates to Rician fading. When $m \leq 1$ Nakagami fading causes more severe performance degradation of signals than Rayleigh fading. So, Nakagami-m distribution can model both Rayleigh and Rician distributions as well as other distributions.

In the case of shadowing there are two important models used in this thesis and these are:

1. **Lognormal Distribution**: This distribution is suitable in modeling the effect of shadowing of the signal due to large-scale environmental obstacles such as tall buildings in RF communications this leads to the local mean power Ω fluctuating about a constant area mean power P_r [30] and this follows a lognormal density as

$$f_\Omega(x) = \frac{1}{x\sqrt{2\pi\sigma^2}}\exp\left(\frac{-\ln^2(x/P_r)}{2\sigma^2}\right) \qquad , x > 0, \tag{2.6}$$

where x is the ratio of transmit-to-receive power which is random and σ is the shadow standard deviation, when $\sigma \to 0$ there is no shadowing. With

further analysis when required using the lognormal distribution becomes complicated, an approximation is used and this is known as the gamma distribution.

2. **Gamma Distribution**: This distribution is used as an approximation [30][31] to the lognormal distribution for analytical tractability with the probability density

$$f_{\Omega}(x) = \frac{1}{\Gamma(m_s)} \left(\frac{m_s}{\Omega_s}\right)^{m_s} x^{(m_s-1)} \exp\left(-x\frac{m_s}{\Omega_s}\right) \qquad x > 0, \quad m_s > 0, \quad (2.7)$$

where m_s is the shadowing severity parameter and Ω_s is the shadow area mean power. The relationships between the lognormal and gamma distribution parameters is discussed in chapter 4.

2.3.4 Channel Coherence Bandwidth and Channel Coherence Time

The channel coherence bandwidth, B_c is a statistical measure of the range of frequencies over which the channel can be considered 'flat' i.e., the estimated maximum bandwidth where two frequencies of a signal are possible to encounter correlated amplitude fading [25]. Two different signals with frequency separation greater than B_c would be affected quite differently in the channel. The channel is said to be flat if B_c is larger than communication signal bandwidth and frequencies that are within a coherence bandwidth of each other are inclined to all fade in a

comparable manner [23].

The channel coherence time T_c is a statistical amount of the time duration where the channel impulse response is almost constant and it quantifies the affinity of the channel response at various intervals. T_c also known as time period where two received signals have an intense possibility for amplitude correlation [25]. If within transmission of a baseband message or communication, the reciprocal bandwidth of the baseband signal is larger than coherence time of transmission channel, distortion occurs at the receiver.

2.4 MIMO System Model

In a conventional MIMO wireless link both the transmitter array antennas N_T and and the receiver array antennas N_R are both connected through a channel where every receive antenna is subjected to a combination of the transmit antennas as shown in the Figure 2.1 below [1]. The channel between the transmitter and receiver antenna pairs is assumed as narrowband time-invariant channel [32][13][17]. The channel coefficient at time l connecting the transmit antenna i and receive antenna j is $h_{ji}(l)$. In lth instant time $x_i(l)$ is transmitted signal from the i_{th} antenna and $y_j(l)$ is the received signal from the j_{th} receive and the noise additive component is $n_j(l)$. $x_i(l)$, $y_j(l)$, and $n_j(l)$ are complex values. N_T signals transmitted shape the input vector signal[2] $\mathbf{x}(l)$ and N_R signals received shape the

[2] a denotes a scalar, $\mathbf{a}$ denotes a vector (column-vector) and $\mathbf{A}$ denotes a matrix.

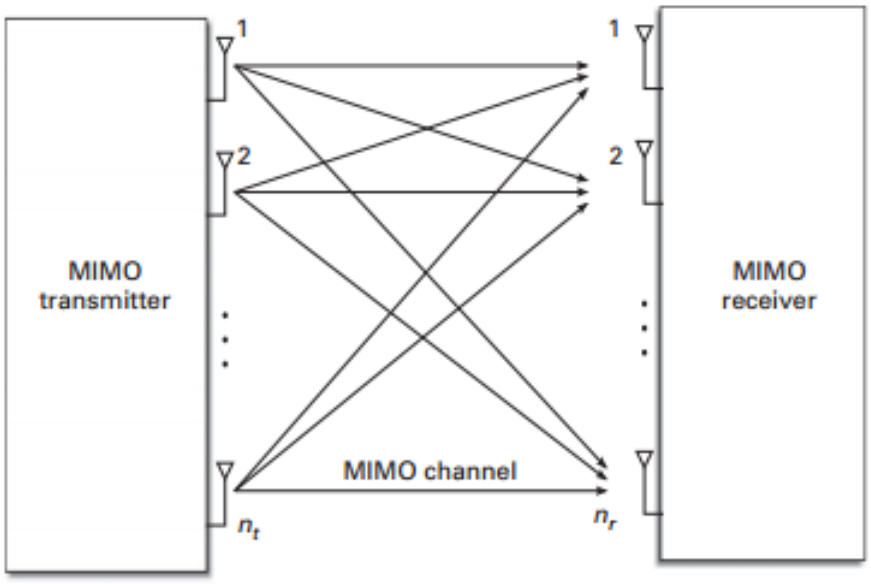

Figure 2.1: MIMO System

output vector signal $\mathbf{y}(l)$. The N_R noise signals shape the noise vector $\mathbf{n}(l)$.

$$\mathbf{x}(l) = \begin{bmatrix} x_1(l) \\ \vdots \\ x_{N_T}(l) \end{bmatrix}, \qquad \mathbf{y}(l) = \begin{bmatrix} y_1(l) \\ \vdots \\ y_{N_R}(l) \end{bmatrix}, \qquad \mathbf{n}(l) = \begin{bmatrix} n_1(l) \\ \vdots \\ n_{N_R}(l) \end{bmatrix}, \tag{2.8}$$

where $n_j(l)$ is a zero mean complex symmetric Gaussian R.V. which is denoted by $n_j(l) \sim \mathcal{CN}\ (0, \sigma_n^2)$ ($\mathcal{CN}$ denotes complex Gaussian zero mean), also the noise at individual receiver antennas have identical variance σ_n^2.

The MIMO channel is described by a matrix $\mathbf{H}(l)$ with dimensions $N_R \times N_T$ given as

$$\mathbf{H}(l) = \begin{bmatrix} h_{1,1}(l) & \cdots & h_{1,N_T}(l) \\ \vdots & \ddots & \vdots \\ h_{N_R,1}(l) & \cdots & h_{N_R,N_T}(l) \end{bmatrix}. \tag{2.9}$$

The MIMO input-output relationship is stated below

$$\mathbf{y}(l) = \sqrt{\rho}\mathbf{H}(l)\mathbf{x}(l) + \mathbf{n}(l), \tag{2.10}$$

where ρ is a scalar which is the SNR of the link. A normalization is assumed to take place where average total transmit power is unity [13], therefore $E\{\|\boldsymbol{x}\|^2\}$ = 1.

2.4.1 Singular Value Decomposition

Singular Value Decomposition (SVD) serves as a tool in mathematics which uses factorization method for matrices and is widely used in signal processing, capacity MIMO measurements, etc. We take an $(N \times M)$ matrix $\mathbf{A}$, the SVD theorem states [15],

$$\mathbf{A} = \boldsymbol{U}\Sigma\,\boldsymbol{V}^H. \tag{2.11}$$

- The eigenvectors of $\boldsymbol{A}\boldsymbol{A}^H$ make up columns of $\mathbf{U} \in \mathbb{C}^{N\times N}$ which is a unitary matrix i.e.$(\boldsymbol{U}\,\boldsymbol{U}^H)= \boldsymbol{I}_N$.

- The singular values in $\Sigma \in \mathbb{R}^{N\times M}$ are square roots of eigenvalues from $\boldsymbol{A}\boldsymbol{A}^H$ or $\boldsymbol{A}^H\boldsymbol{A}$. The singular values are the diagonal entries of the Σ matrix and are arranged in descending order.

- The eigenvectors of $\boldsymbol{A}^H\boldsymbol{A}$ make up the columns of $\mathbf{V}$. $\mathbf{V} \in \mathbb{C}^{M\times M}$ which is a unitary matrix i.e.$(\boldsymbol{V}\,\boldsymbol{V}^H)= \boldsymbol{I}_M$.

Calculating the SVD of the MIMO channel matrix $\mathbf{H}$ leads to the following factorization

$$\mathbf{H} = \boldsymbol{U}\Sigma\,\boldsymbol{V}^H, \tag{2.12}$$

where $\boldsymbol{U}$ is an $\boldsymbol{N}_R \times r$ matrix , $\boldsymbol{V}$ is an $\boldsymbol{N}_T \times r$ and Σ is an $r \times r$ diagonal matrix with diagonal elements the singular values $\sigma_1, \sigma_2, ..., \sigma_r$ of the channel. The column vectors of matrices $\boldsymbol{U}$ and $\boldsymbol{V}$ are orthonormal. $\boldsymbol{U}\,\boldsymbol{U}^H = \boldsymbol{I}_r$ and $\boldsymbol{V}\,\boldsymbol{V}^H = \boldsymbol{I}_r$, where $\boldsymbol{I}_r$ is the $r \times r$ identity matrix. Using Eqn.(2.12) $\mathbf{H}$ can be substituted into Eqn.(2.10) using this decomposition, hence the received signal becomes in Eqn.(2.10)

$$\mathbf{y} = \boldsymbol{U}\Sigma\,\boldsymbol{V}^H\boldsymbol{x} + \boldsymbol{n}, \tag{2.13}$$

by setting $\mathbf{y}' = \boldsymbol{U}^H\mathbf{y}$, $\mathbf{x}' = \boldsymbol{V}^H\mathbf{x}$ and $\mathbf{n}' = \boldsymbol{U}^H\mathbf{n}$, Eqn.(2.10) can be rewritten as

$$\mathbf{y}' = \Sigma\mathbf{x}' + \mathbf{n}', \tag{2.14}$$

where $y' = [y'_1\ ,...,\ y'_{N_R}]^T$, $x' = [x'_1,...,\ x'_{N_T}]^T$, $\Sigma = diag(\sqrt{\lambda_1}, .., \sqrt{\lambda_R}, 0, ...0)$ and $r = min(N_R, N_T)$ denotes the rank of the channel matrix.

2.4.2 MIMO Capacity based on CSI known at both Transmitting and Receiving sides (Perfect CSI)

When the channel matrix $\mathbf{H}$ is only known at the receiving antennae, the transmitter allocates equal power to the signals transmitted on the multiple transmit antennas [14], but when the channel matrix is known to both receiver and

transmitter, the transmitter allocates transmitted power more efficiently and thus achieve higher rates [15][1]. With available CSI at both receiver and transmitter an optimal power allocation could be exploited, this is called the water-filling technique [16]. The main idea of water-filling strategy is allocation of increased power to improve performance in sub-channels with higher SNR this maximizes the data transmission in sub channels where power allocation in each sub-channel is related to data rate using the Shannon Gaussian capacity formula [14][16].

A MIMO wireless channel with N_T transmit and N_R receive antennas in a frequency-non selective channel is considered, the channel matrix $\mathbf{H}$ is of rank r, $\mathbf{H}$ can be represented from Eqn.(2.12) and since $\mathbf{H}$ is known at both receiver and transmitter sides, the transmitted signal vector of dimension $r\times$ 1 is pre-multipled by matrix $\boldsymbol{V}$ and the received signal is pre-multipled by the matrix $\boldsymbol{U}^H$ therefore [18],

$$\boldsymbol{x}_v = \boldsymbol{V}\boldsymbol{x} \quad and \qquad \mathbf{y}' = \boldsymbol{U}^H\mathbf{y} \ . \tag{2.15}$$

The transmitted signal vector $\boldsymbol{x}$ has zero-mean, complex-valued Gaussian elements. A constraint is placed such that the sum of the variances of the elements in $\boldsymbol{x}$ is to be equal to N_T i.e. $E\ (x^H x)= \sum_{k=1}^{r} E[|x_k|^2] = \sum_{k=1}^{r} \sigma_{kx}^2 = N_T$.

Therefore the signal transmitted on the N_T antennas is $\sqrt{\frac{E_S}{N_T}}\boldsymbol{V}\boldsymbol{x}$, the received signal vector is written as

$$\boldsymbol{y} = \sqrt{\frac{E_S}{N_T}}\mathbf{H}\boldsymbol{V}\boldsymbol{x} + \boldsymbol{n}\boldsymbol{y} = \sqrt{\frac{E_S}{N_T}}\boldsymbol{U}\Sigma\boldsymbol{x} + \boldsymbol{n} \ . \tag{2.16}$$

The signal vector $\boldsymbol{y}$ is pre-multiplied by $\boldsymbol{U}^H$ and the transformed $r \times 1$ to obtain

$$\mathbf{y}' = \boldsymbol{U}^H \boldsymbol{y} = \sqrt{\frac{E_S}{N_T}} \Sigma \boldsymbol{x} + \mathbf{n}' \ . \tag{2.17}$$

It can be observed that the channel characterized by $N_R \times N_T$ channel matrix is equivalent to r decoupled SISO (Single-Input Single-Output) channels [18] whose output is

$$y' = \sqrt{\frac{E_S \lambda_k}{N_T}} x_k + n'_k, \qquad k = 1, 2, .., r \ . \tag{2.18}$$

Therefore the capacity of a MIMO channel for a specific power allocation at the transmitter is given as [18]

$$C(\{\sigma_{kx}^2\}) = \sum_{k=1}^{r} \log_2 \left(1 + \frac{E_s \lambda_k}{N_T N_0} \sigma_{kx}^2 \right) \ . \tag{2.19}$$

It can be noted that the energy transmitted per symbol on the kth sub channel is $\frac{E_s}{N_T} \sigma_{kx}^2$, the transmitter allocates total transmitted power across the N_T antennas so as to maximize $C(\{\sigma_{kx}^2\})$, therefore the capacity of a MIMO channel in optimum power allocation is stated as [18][15],

$$C = max_{\{\sigma_{kx}^2\}} \sum_{k=1}^{r} \log_2 \left(1 + \frac{E_s \lambda_k}{N_T N_0} \sigma_{kx}^2 \right) \ . \tag{2.20}$$

The above Eqn.(2.20) solution satisfies the "*water- filling principle*" which allocates more power to sub channels which have low noise power, i.e., according to the ratio $\frac{N_0}{\lambda_k}$ less power to sub channels that have high power.

2.4.3 MIMO Capacity based on CSI known at the Receiver

A flat fading MIMO channel is characterized by channel matrix **H** from Eqn.(2.12) with N_T transmit antennas and N_R receive antennas, where $\boldsymbol{x}$ is the signal vector transmitted is fixed with a zero mean and auto-covariance matrix $\boldsymbol{R}_{xx}$, and the received signal vector $\boldsymbol{y}$ is expressed is already in Eqn.(2.10) and $\boldsymbol{n}$ is the zero-mean Gaussian noise received vector with covariance matrix $\boldsymbol{R}_{nn} = N_0 \boldsymbol{I}_{N_R}$. Even though **H** is a random matrix realization, it is treated as deterministic and the receiver has a knowledge of it. From [17][18] the capacity is written as

$$C = max_{tr(R_{xx})=E_S} \log_2 det \left(\boldsymbol{I}_{N_R} + \frac{1}{N_0} \boldsymbol{H} \boldsymbol{R}_{xx} \boldsymbol{H}^H \right) bps/Hz \ , \tag{2.21}$$

and $tr(R_{xx})$ is the trace of signal covariance $\boldsymbol{R}_{xx}$. In the event that the signals in the transmitter are independent symbols and their energy per symbol is $\frac{E_S}{N_T}$, with a diagonal covariance matrix i.e. $\boldsymbol{R}_{xx} = \frac{E_s}{N_T} \boldsymbol{I}_{N_T}$ and trace $(\boldsymbol{R}_{xx}) = E_s$.

The capacity of Eqn.(2.21) simplifies to

$$C = \log_2 det \left(\boldsymbol{I}_{N_R} + \frac{E_s}{N_0 N_T} \boldsymbol{H} \boldsymbol{H}^H \right) bps/Hz \ . \tag{2.22}$$

Using the eigenvalues of $\boldsymbol{H}\boldsymbol{H}^H$ by using the eigenvalue decomposition $\boldsymbol{H}\boldsymbol{H}^H = \boldsymbol{Q}\Lambda\boldsymbol{Q}^H$, the capacity rewritten as [18],

$$\begin{aligned} C &= \log_2 det\left(\boldsymbol{I}_{N_R} + \tfrac{E_s}{N_0 N_T}\boldsymbol{Q}\Lambda\boldsymbol{Q}^H\right) \\ &= \log_2 det\left(\boldsymbol{I}_{N_R} + \tfrac{E_s}{N_0 N_T}\boldsymbol{Q}^H\boldsymbol{Q}\Lambda\right) \\ &= \log_2 det\left(\boldsymbol{I}_{N_R} + \tfrac{E_s}{N_0 N_T}\Lambda\right) \\ &= \textstyle\sum_{i=1}^{r} \log_2 det\left(\boldsymbol{I}_{N_R} + \tfrac{E_s}{N_0 N_T}\lambda_i\right) \end{aligned} \quad , \tag{2.23}$$

where λ_i are the eigenvalues of Λ.

2.4.4 MIMO Capacity with Partial Transmit Channel Knowledge

Sometimes the transmitter doesn't obtain the immediate knowledge of the channel information, although it can have a incomplete knowledge known as the statistics of $\mathbf{H}$. Since the transmitter has no information of $\mathbf{H}$ it is impossible to modify the input covariance matrix at all-time instants, but it is feasible to assign power in a stochastic way [1][15][27], by distributing power to the eigendirections which are strong in average. The ergodic capacity of a MIMO channel using channel distribution information at the transmitter ($CDIT$) is [18]

$$\bar{C}_{CDIT} \triangleq \bar{C} = max_{\mathbf{R}_{xx}\geq 0: Tr\{R_{xx}\}=1} E\{\log_2 det[\boldsymbol{I}_{N_R} + \rho\boldsymbol{H}\mathbf{R}_{xx}\boldsymbol{H}^H]\} \ , \tag{2.24}$$

where $\mathbf{R}_{xx}$ is optimized to give a maximum ergodic mutual information.

2.4.5 Ergodic Capacity

Without CSIT, dependable communication is still possible using coding over an vast number of asymptotic channel coherence time, by even-out fading in the channel. Using the CSIT, a maximum rate (R) for dependable communication can be achieved and when R happens to be consistent over channel fading it is known as the *ergodic* capacity [7][15]. An average is taken of the capacity in the deterministic channel over the statistics of the channel matrix and is used to determine the ergodic capacity.

The ergodic capacity for a MIMO channel can be obtained as an average expression over the joint probability density function of the eigenvalues $\{\lambda_i\}$ of the channel matrix $\mathbf{H}$ [18], therefore ergodic capacity is given as

$$\begin{aligned} \bar{C}_{MIMO} &= E\left\{\sum_{i=1}^{r} \log_2\left(1+\frac{E_s}{N_0 N_T}\lambda_i\right)\right\} \\ &= \int_0^\infty ... \int_0^\infty [\sum_{i=1}^{r} \log_2\left(1+\frac{E_s}{N_0 N_T}\lambda_i\right)] p(\lambda_i, ..., \lambda_r) d\lambda_i, ..., d\lambda_r \end{aligned} \quad . \quad (2.25)$$

The ergodic capacity of some MIMO configurations under Rayleigh fading are shown in Figures 2.2, 2.3 and 2.4.

2.4.6 Outage Capacity

For a non-ergodic channel when the channel stays constant and $\mathbf{H}$ can be held fixed for all the uses of the channel, the channel fades cannot be estimated and it is difficult to promise dependable communication. Instead of using the Shannon capacity [27], a useful performance metric is known as Outage probability. It is

the probability that the capacity *C(h)* is below some value for a specified threshold capacity C_{out} [26]. The channel is assumed to be quasi-static for the duration of a frame of data, but the channel matrix may change from frame to frame. The outage probability is expressed as [18],

$$P_{out} = P_r(C(h) \leq C_{out}) \ , \tag{2.26}$$

the above equation (2.20) can be expanded as

$$\begin{aligned} P_{out}(C_{out}) &\triangleq P_r\left(log_2(1 + SNR|h|^2) < C_{out}\right) \\ &= P_r\left(|h|^2 < \tfrac{2^{C_{out}}-1}{SNR}\right). \end{aligned} \tag{2.27}$$

2.4.7 Capacity plots for Conventional MIMO Systems

The capacity plots are shown below for SIMO systems (Figure 2.2).(where $N_T = 1$ and $N_R \geq 1$), MISO systems (Figure 2.3) (where $N_R = 1$ and $N_T \geq 1$) and are compared to the MIMO system (Figure 2.4), it can be seen that as the number of transmit and receive antennas increase the capacity of the MIMO system increases tremendously as compared to the SIMO and MISO systems. Therefore at high SNRs, the capacity increases linearly with the number of antenna pairs.

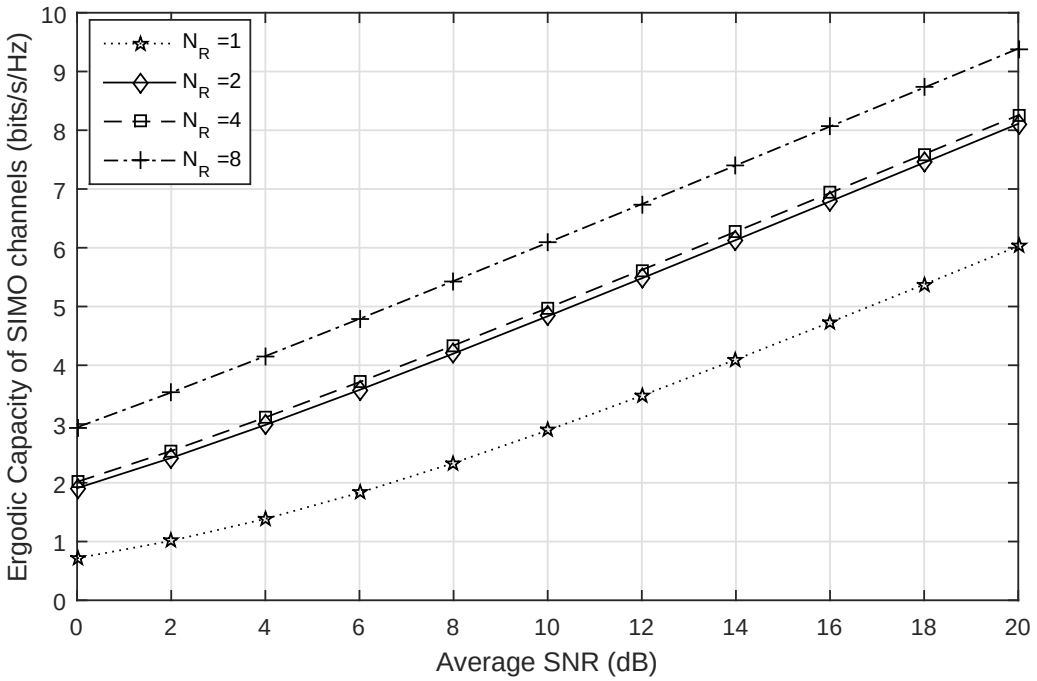

Figure 2.2: Ergodic Capacity for SIMO system.

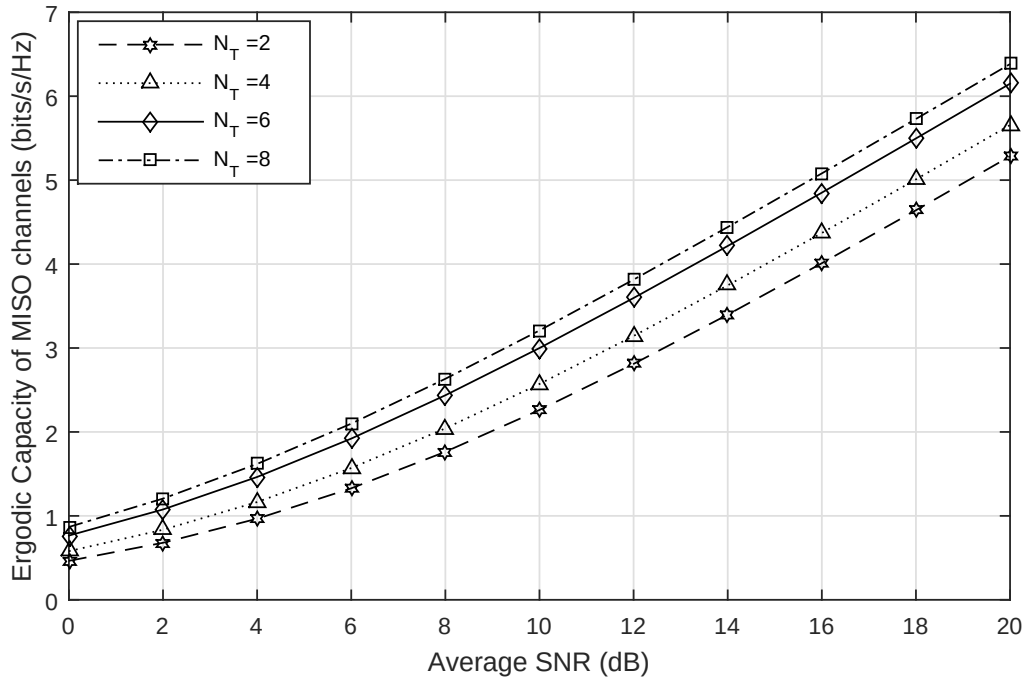

Figure 2.3: Ergodic Capacity for MISO system.

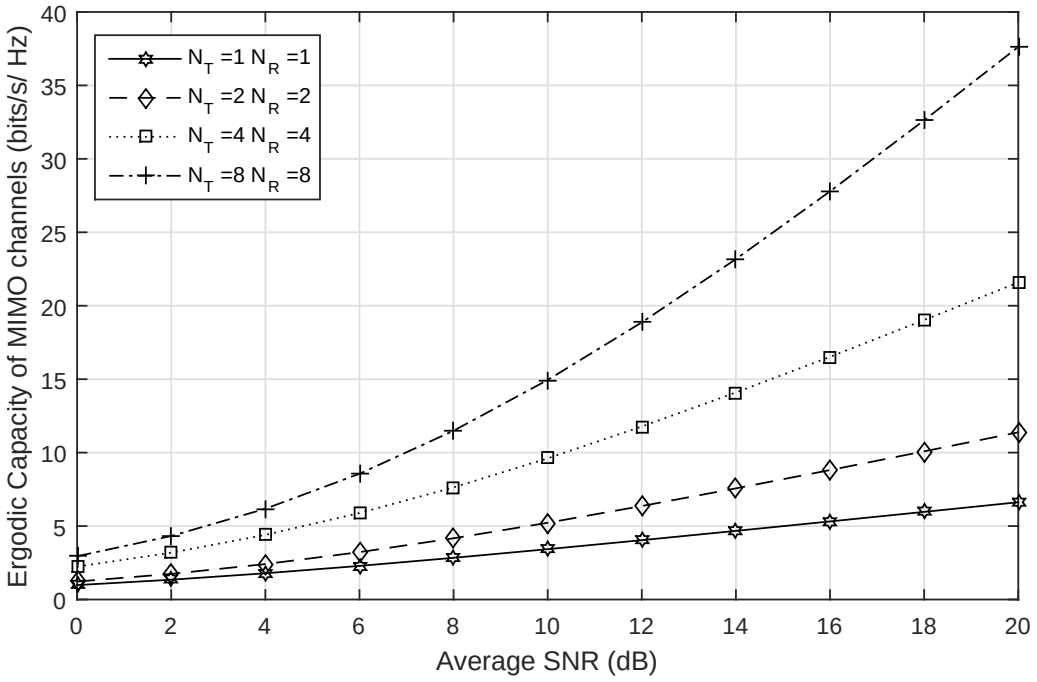

Figure 2.4: Ergodic Capacity for MIMO system.

2.5 MIMO Detection

Low complexity signal processing schemes or algorithms are used for synchronization, channel estimation, precoding, signal detection and channel decoding, these play a key role in the practical implementation of MIMO systems [32][7]. The job of MIMO detector at the receiver is to recover the symbols that are transmitted simultaneously from multiple transmitting antennas and can sometimes be a bottle neck in terms of overall performance and complexities. Detectors can generally be classified as Maximum likelihood, Linear and Nonlinear detectors.

2.5.1 Maximum Likelihood Detector (MLD)

The MLD is the optimum detector because it minimizes error probability, the additive noise terms at the N_R receiving antennas are i.i.d and zero mean Gaussian therefore the joint conditional PDF $\boldsymbol{(y|x)}$ is also Gaussian at every phase, the receiver makes use of ML decoding to detect effectively transmitted vector symbols i.e., it selects the vector $\hat{x}$ that minimizes the Euclidean distance metric [18]

$$\mu(x) = \sum_{m=1}^{N_R} |y_m - \sum_{n=1}^{N_T} h_{mn} x_n|^2 \ . \tag{2.28}$$

2.5.2 Linear Detectors

The principle of such detectors is processing the received signal vector $\mathbf{y}$ through a linear filter $\mathbf{W}$ at every instant k, such that the combined channel matrix $\mathbf{WH}$ equates to a diagonal matrix [15], which enables the individual detection of each of the N_T components of $\mathbf{z}$ using a decoder [18],

$$\mathbf{z} = \mathbf{Wy} = \sqrt{\frac{E_s}{N_T}} \mathbf{WHx} \ + \mathbf{Wn} \ . \tag{2.29}$$

The following receivers (detectors) use this principle in literature namely:

1. *Maximal Ratio Combining Receivers*: In exploiting spatial diversity that is provided by MIMO systems, a desirable design is to choose weighting factors which maximizes the receive SNR and minimizes the outage probability. MRC obtains weights that maximizes the output of the SNR, this makes it

optimal in terms of SNR. The received signal at the array elements using Eqn.(2.10) in vector form is stated as

$$z = \mathbf{w}^H \mathbf{y} = \mathbf{w}^H \mathbf{H}\mathbf{x} + \mathbf{w}^H \mathbf{n}, \tag{2.30}$$

because the average power of the input signal is unity, the instantaneous output SNR can be written as [33],

$$\gamma = \frac{|\mathbf{w}^H \mathbf{h}|^2}{\mathbb{E}\{|\mathbf{w}^H \mathbf{n}|^2\}}. \tag{2.31}$$

The denominator noise power is given as

$$\begin{aligned} P_n &= \mathbb{E}\{|\mathbf{w}^H \mathbf{n}|^2\} = \mathbb{E}\{|\mathbf{w}^H \mathbf{n}\mathbf{n}^H \mathbf{w}|\}, \\ &= \mathbf{w}^H \mathbb{E}\{\mathbf{n}\mathbf{n}^H\}\mathbf{w} = \sigma^2 \mathbf{w}^H \mathbf{I}_N \mathbf{w}, \\ &= \sigma^2 \mathbf{w}^H \mathbf{w} = \sigma^2 \|\mathbf{w}\|^2, \end{aligned} \tag{2.32}$$

where $\mathbf{I}_N$ is an $N \times N$ identity matrix, $\mathbf{w}$ is scaled such that $\|\mathbf{w}\| = 1$, therefore the SNR is rewritten as

$$\gamma = \frac{|\mathbf{w}^H \mathbf{h}|^2}{\sigma^2}, \tag{2.33}$$

by using the Cauchy-Schwarz inequality, the above Eqn.(2.32) becomes max-

imum when $\mathbf{w}$ is linearly proportional to $\mathbf{h}$ i.e.

$$\mathbf{w} = \mathbf{h}, \tag{2.34}$$

therefore the SNR reduces to

$$\gamma_{MRC} = \frac{|\mathbf{h}^H\mathbf{h}|^2}{\sigma^2\mathbf{h}^H\mathbf{h}} = \frac{\mathbf{h}^H\mathbf{h}}{\sigma^2} = \sum_{i=1}^{N-1}\frac{|h_i|^2}{\sigma^2} = \sum_{i=1}^{N-1}\gamma_i. \tag{2.35}$$

The MRC SNR output is the sum of the received SNRs at all antennas. The MRC can achieve the maximum SNR among all the linear combining techniques [34].

2. *Zero- Forcing Receivers (ZF)*: The *ZF* receiver inverts the channel matrix and suppresses interference induced by the other antennas. It forms an estimate of $\boldsymbol{x}$ by linearly combining the received signals $\{y_m, 1 \leq m \leq N_R\}$, the weighting matrix $\mathbf{W}$ is selected so that the inter-channel interference is completely eliminated by setting $N_T = N_R$ by setting $\mathbf{W}^H = \mathbf{H}^{-1}$ [18],

$$\hat{\mathbf{x}} = \mathbf{H}^{-1}y = x + \mathbf{H}^{-1}n \ . \tag{2.36}$$

Each element of the estimate $\hat{\mathbf{x}}$ is then quantized to the closet transmitted symbol value. The estimate is not corrupted by inter-channel interference, but it does not exploit the signal diversity inherent in received signal [18]. The output of *ZF* is only a function of the symbol vector to be detected and

the noise, when $N_R > N_T$ the weighting matrix $\mathbf{W}$ can be selected as pseudo inverse of the channel matrix as

$$\mathbf{W}^H = (\mathbf{H}^H\mathbf{H})^{-1}\mathbf{H}^H \ . \tag{2.37}$$

3. *Minimum Mean Squared Error (MMSE) Receiver*: The MMSE detector minimizes the combination of noise and interference but doesn't fully remove interference from other antennas. It does this by combining the received signals $\{y_m, 1 \leq m \leq N_R\}$ to form an estimate of the transmitted symbols $\{x_n, 1 \leq n \leq N_T\}$, the linear combination is written in matrix form as [18],

$$\hat{x} = \mathbf{W}^H\mathbf{y} \ , \tag{2.38}$$

where $\mathbf{W}$ is an $N_R \times N_T$ weighting matrix, which is selected to minimize the mean square error

$$J(\mathbf{W}) = E[\|\mathbf{e}\|^2] = E[\|\mathbf{x} - \mathbf{W}^H\mathbf{y}\|^2] \ , \tag{2.39}$$

the minimization of $J(\boldsymbol{W})$ leads to the solution for the optimum weight vectors $\mathbf{w}_1, \mathbf{w}_2, ..., \mathbf{w}_{N_T}$ as $\mathbf{w}_n = \mathbf{R}_{yy}^{-1}\mathbf{r}_{x_n y}$, where $n = 1, 2, ...N_T$ [18],

$$R_{yy} = E[\mathbf{y}\mathbf{y}^H] = \mathbf{H}\mathbf{R}_{xx}\mathbf{H}^H + N_0\mathbf{I} \ , \tag{2.40}$$

where $\mathbf{R}_{yy}$ is the auto correlation matrix ($N_R \times N_R$) of the received signal

vector $\mathbf{y}$ and,

$$\mathbf{R}_{xx} = E[\mathbf{x}\mathbf{x}^H] \text{ and } \mathbf{r}_{x_n y} = E[x_n^* \mathbf{y}] \ , \tag{2.41}$$

when the signal vector has uncorrelated and zero-mean components $\mathbf{R}_{xx}$ is a diagonal matrix and N_0 is the noise in the channel.

2.6 Previous Work on Large-scale MIMO Systems

2.6.1 Going Large: Large-scale MIMO Systems

Massive MIMO is also called large MIMO or large-scale MIMO, these are MIMO systems that use tens to hundreds of array antennas in their communication terminals. Different MIMO systems configurations can be used depending on the application scenario, these include Point-point MIMO and Multi-User (MU) MIMO configurations. For the MU-MIMO we have both point-to-multipoint (e.g. downlink in cellular systems) and multipoint-to-point MIMO (e.g. uplink in cellular systems). Large-scale MIMO systems involves using a large number of antennas simultaneously serving a smaller number of terminals, this inequality in numbers emerges as a favorable performance condition and also a practical one. The amount of terminals that can be served simultaneously is limited by the inability to acquire the CSI for an unlimited number of terminals [13][32]. A typical application scenario for point-to-point large MIMO configuration is providing high-speed

wireless backhaul connectivity between BS using multiple antennas at each BS.

Also in MU-MIMO the communication is between the base station and multiple user terminals, where the user terminals can be small devices like smart phones or medium terminals like laptops or set-up boxes, but for user terminals like the smart phones, only a limited number of antennas can be mounted due to space constraints but in devices like setup boxes or laptops, a larger number of antennas can be used at the user terminal. The use of tens to hundreds of antennas at the base station end is not too difficult to implement, and the greater number of antennas at the base station the greater the spatial degrees of freedom available to perform precoding on the downlink and detection on the uplink [7][35].

Using conventional time and frequency division multiplexing via orthogonal frequency division multiplexing (OFDM), larger number of terminals can be accommodated by using this methods, large-scale MIMO is a new research field both in communication theory and propagation. The underlying reason behind large-scale MIMO systems is to reap all the benefits of conventional MIMO systems, but on a wider scale[36], the larger the number of BS receive antennas, the larger the number of uplink users that can be supported in the system [26] and in the multiuser downlink when a large number of transmit antenna is available at the base station it allows for simple precoding methods and flexible user scheduling.

A distinguishing feature stated in [8] of large-scale MIMO systems is that a large number of service-antennas work for a significant smaller number of autonomous antennas which allows simplest multiplexing pre-coding and de-coding algorithms

to be optimal. The law of large numbers helps in facilitating power-control and resource allocation in such systems. In [9], the promise benefits of using large-scale MIMO systems in 5G implementation is stated as providing enhancements in spectral efficiency, power efficiency improvements, and channel responses are smoothed out as all small- scale randomness reduces as channel observations increases. For a number of active users orthogonality is sharpened as the number of BS antennas increases and linear transceivers perform more optimally.

In [37] large-scale MIMO systems is stated as an enabling technology for 5G and future networks in improving the peak rate and also increasing system capacity of cellular networks. It also states that developments in antenna implementation now supports active antenna element whereby the antenna element can dynamically form a beam in a vertical or tilt domain, which is known as 3D MIMO. This provides better coverage and also improves throughput in the areas when users are distributed in different areas of buildings. In [21] a proposal to use large-scale MIMO systems to combat interference and improve the rank of the overall channel matrix is stated.

Some additional benefits of large-scale MIMO systems is no extra site cost, it supports cell-wide and intercell load balancing which provides an increase in signal processing at a single site. Also adding more antennas at macro cells is a viable option in future 5G systems. The authors in [38] state that in designing 5G mobile networks architectures and using high frequency bands in large-scale MIMO antenna arrays with small form factors, the capacity can have a 10-fold

increase when compared with conventional antenna systems and also it exploits beamforming gain to extending the coverage of higher frequencies which suffer from line-of sight attenuation. Large-scale MIMO systems is also used to provide high-capacity wireless backhaul and fronthaul links in LOS conditions.

2.6.2 Channel Capacity

The initial work done in [27] and [14] on conventional MIMO channel capacity laid the foundation for large-scale MIMO systems. The work provides summaries of the ergodic capacity against the outage capacity for single-user MIMO channels, and also results for MIMO broadcast channels and multiple-access channels (MAC). They show that the CSI plays an important function in calculating capacity. The research of [39] uses the large dimensional random matrix theory to derive deterministic equivalent ergodic sum rate and also an algorithm for large-scale MIMO systems with LOS components, the work is extended in [40] which considered relay- assisted MIMO cellular system, where two asymptotic sum rate expressions is derived for large MIMO cellular systems for both a fixed number of users and a large number of users respectively.

The ergodic capacity of MIMO systems operating in generalized-K fading conditions is part of the work done in [41] using the Walsh matrix theory, an analytical capacity bound is also derived for arbitrary values of the SNR with a number of antenna elements using majorization theory. The research of [24] looks into fading correlation for multi-antenna systems, part of the research done shows how fading

correlations affect the capacity, and also the fading depends on the physical parameters of the antennas and the scatter characteristics. The findings show that fading correlation can potentially lead to lower capacity than using i.i.d fading assumptions. In [42] a new stochastic MIMO channel model was developed to be able to predict capacity better and also improves spatial channel structure. The research makes use of joint correlation properties of the receiver and the transmitter.

The work in [43] makes use of random matrix and free probability theory to derive a closed form expression of channel capacity for MIMO systems over composite fading channels. Part of the work done in [44] deals with deriving upper and lower capacity bounds, which was based on having perfect CSI for the downlink and imperfect pilot-based CSI estimation for the uplink in large-scale MIMO with non-ideal hardware. The research of [45] was interested in non-cooperative multi-cell multi-user TDD (Time-division duplexing) systems. Tight approximations of achievable rate for such systems was derived under imperfect channel estimation and terminal-specific antenna correlation. Some of the results was applied to large distributed antenna systems.

The research of [12] provided new sum rate bounds for MRC, ZF and MMSE for perfect and imperfect CSI and how increase in antennas affect both spectral and energy efficiency when compared to a single-antenna system. The research in [12] was extended to [46] where power scaling for uplink massive mimo systems was researched into. They showed that the transmit power of users can also be

reduced without affect the performance of the communication on link.

2.6.3 Beamforming

Beamforming (BF) is a powerful technique which increases the link SNR through focusing the energy into desired directions. By BF, the transmit and receive antenna patterns can be focused into a specific angular direction by using an appropriate choice of complex baseband antenna weights, the more correlated the antenna signals, the better the BF, under LOS channel conditions, the receiver and transmitter gains may add up, which leads to an upper limit of N_T and N_R for the beamforming gain of a MIMO system where N_T and N_R is the number of transmit and receive antennas respectively .

The beamforming for large-scale MIMO systems was considered in [47] which investigated the performance of unconstrained size antenna arrays when the effects of far-field clustering scatters are considered and the average beamforming gain to understand beamforming performance of large scale antennas, the results show that beamforming gain grows with a decreasing rate as more antennas are added, specially for non-zero angle spread channels, the work done in [48] considers the problem of distributed transmit beamforming to a distant destination using explicit feedback it was found that explicit feedback does not scale too well for distributed MIMO. The research shows that distributed receive beamforming using amplify-forward relays can be used to create spatial degrees of freedom. In [45] part of the work done involves using beamforming to determine how many

antennas are needed to achieve performance of both the MMSE and regularized ZF processing. Using beamforming in the downlink, asymptotic tight approximation of achievable rate is derived in this paper.

A part of the work done in [35] uses beamforming training for channel estimation to acquire CSI at each user, by allowing the base station to precode pilot sequences and forward to all users. The beamforming training employs using both maximum-ratio transmission and ZF precoding techniques and compares the performances. Also a simpler zero-forcing beamforming scheme was proposed in [49] which was based on sparse matrix inversion, it was designed to work in a two dimensional network where a large number of antenna elements are deployed uniformly in an $m \times m$ grid to cover large public venues.

A significant contribution of this paper using a matrix inversion algorithm to reduce complexity of the zero-forcing beamforming in distributed large-scale MIMO system while keeping a negligible throughput loss. This research was extended to [50], a part of the research done in [51] involves using beamforming schemes to maximize large-scale MIMO, this is done by transmitting continuous precoding matrix indicator (PMI) feedback signals through a series of patterns. Communication systems use PMI to report the CSI to the enhanced node B (eNB), this increases feedback overhead as the number of antennas increases, the beamforming schemes deployed solves this by implementing CSI reports and a codebook extension.

In [52] the research is based on the performance analysis of zero-forcing beam-

forming when used in a finite-antenna large-scale MIMO system which employs a time-shifted pilot scheme. The time shifted pilot scheme is used to combat pilot contamination using infinite base station antennas and using conjugate beamforming, some mathematical expressions for sum-rate lower bounds and the signal-to-interference ratios (SINR) of both the forward and reverse links is provided.

CHAPTER 3

CAPACITY OF LARGE-SCALE MIMO OVER MULTIPATH FADING CHANNELS

3.1 Large-Scale MIMO Uplink Model

For the system model, the MU-MIMO uplink is used. In this system as shown in Figure (3.1) there is one BS that is equipped with M antenna arrays which receives signal vectors from K single-antenna users [12]. In this model[3], users transmit data using identical time-frequency resource, the received $M \times 1$ vector at the BS is

$$\mathbf{y} = \sqrt{p_u}\boldsymbol{S}\boldsymbol{x} + \boldsymbol{n} \quad , \tag{3.1}$$

where $\mathbf{S}$ is a representation of the $M \times K$ channel matrix between both the

[3]In previous chapter ρ was used to represent SNR, but p_u is used for this model.

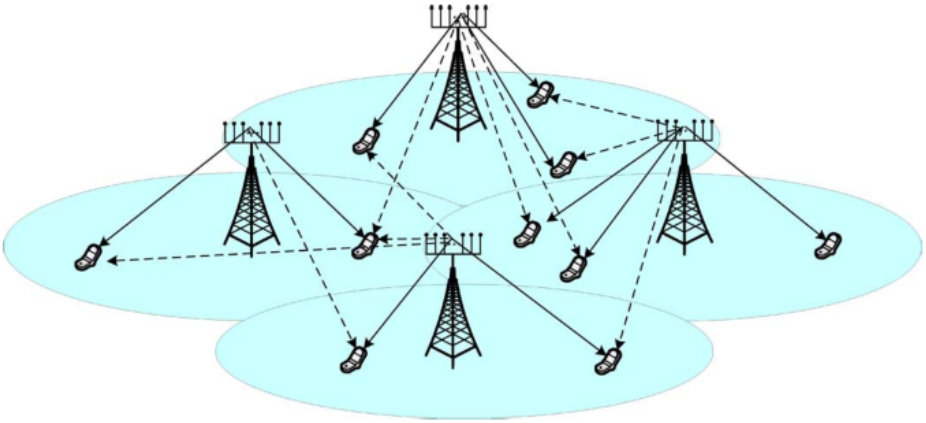

Figure 3.1: Multi-User large-scale MIMO System

BS and the K users. $s_{mk} \triangleq [\mathbf{S}]_{mk}$ is the channel coefficient linking the mth antenna of the BS and the kth user. The vector of symbols transmitted by K users simultaneously is $\sqrt{p_u}\mathbf{x}$, p_u is the mean transmitted individual user power and $\boldsymbol{n}$ is a Gaussian noise vector $\sim \mathcal{CN}\ (0,\ \sigma_n^2)$. The variance of the noise vector is set to unity, p_u is the normalized transmit SNR and has no dimension. The channel matrix $\boldsymbol{S}$ is modeled as independent fast fading, large-scale fading and log-normal shadowing. The coefficients of the channel matrix s_{mk} is written as

$$s_{mk} = h_{mk}\sqrt{\gamma_k}, \qquad m = 1, 2, ..., M \qquad k = 1, 2, ..., K, \tag{3.2}$$

where h_{mk} models fast fading parameter from the desired user to the antenna of the BS. $\sqrt{\gamma_k}$ models both path-loss and shadowing and is presumed to be already known and is independent over m and is held constant in this section [35]. This presumption holds because the distances separating users and the BS is far greater than the distance in-between the antennas, therefore the γ_k parameter

doesn't vary quickly in time. The channel matrix **S** can be written as

$$\boldsymbol{S} = \boldsymbol{H}\Gamma_s^{\frac{1}{2}} \ , \tag{3.3}$$

$\boldsymbol{H}$ is defined as the $M \times K$ matrix of fast fading elements linking the K users with the BS, its coefficients is given as $[\boldsymbol{H}]_{mk} = h_{mk}$, and Γ_s is $K \times K$ diagonal matrix and $[\Gamma_s]_{kk} = \gamma_k$.

In matrix notation the channel matrix **S** is modeled as

$$\mathbf{S} = \begin{bmatrix} h_{1,1}\sqrt{\gamma_k} & \cdots & h_{1,k}\sqrt{\gamma_k} \\ \vdots & \ddots & \vdots \\ h_{m,1}\sqrt{\gamma_k} & \cdots & h_{m,k}\sqrt{\gamma_k} \end{bmatrix} \qquad m = 1, 2, ..., M \ , \qquad k = 1, 2, ..., K. \tag{3.4}$$

3.2 Achievable and Asymptotic Rates for Multipath Fading Channels

In [12], the achievable rate for the Rayleigh fading was derived for the desired user in a large-scale MU-MIMO system. This section extends that work when the desired user experiences Rician fading. As the number of antennas at the BS grows large, the transmit power of users can be reduced, and a good Quality of Service (QOS) can still be maintained. New achievable rates are derived for the uplink in the BS. In theory MLD can be used to obtain optimal performance of the BS, but because the complexity of the detector increases exponentially with K, other detectors are used as M and K become large, although M is considerably

greater than K i.e., $M \gg K \gg 1$, the detectors used are *MRC*, *ZF* and *MMSE* which perform well [11] in reported literature. The MRC is used in this section and the case of perfect CSI is only considered.

3.2.1 Capacity Bounds for Full CSI at the Receiver

With the BS having perfect CSI, i.e., the channel matrix $\boldsymbol{S}$ is known, $\boldsymbol{W}$ is a $M \times K$ linear detector matrix which depends on $\boldsymbol{S}$, the signal received can be split into different data outflows by using the linear detector and it is multiplied with $\boldsymbol{W}^H$ in [33][46],

$$\boldsymbol{r} = \boldsymbol{W}^H \boldsymbol{y} \ . \tag{3.5}$$

For the MRC linear detector from [33],

$$\boldsymbol{W} = \boldsymbol{S} \ , \tag{3.6}$$

by combining both Eqn.(3.1) and Eqn.(3.5) the vector received using a linear decoder is

$$\boldsymbol{r} = \sqrt{p_u}\, \boldsymbol{W}^H \boldsymbol{S} \boldsymbol{x} + \boldsymbol{W}^H \boldsymbol{n} \ , \tag{3.7}$$

letting both r_k and x_k be the kth elements of $K \times 1$ vectors $\mathbf{r}$ and $\mathbf{x}$, respectively using this new notation in Eqn.(3.7) we have

$$r_k = \sqrt{p_u} \boldsymbol{w}_k^H \boldsymbol{s}_k x_k + \sqrt{p_u} \sum_{i=1, i \neq k}^{K} \boldsymbol{w}_k^H \boldsymbol{s}_i x_i + \boldsymbol{w}_k^H \boldsymbol{n} \ , \tag{3.8}$$

where $\sqrt{p_u}\sum_{i=1,i\neq k}^{K}\boldsymbol{w}_k^H\boldsymbol{s}_i x_i$ is due to interferers, both $\boldsymbol{w}_k$ *and* $\boldsymbol{s}_k$ are the kth columns of matrices $\boldsymbol{W}$ and $\boldsymbol{S}$ respectively. Assuming an ergodic channel, the achievable uplink rate for the kth user is given by [53] [12],

$$R_{P,k} = \mathbb{E}\left\{\log_2\left(1+\frac{p_u|\mathbf{w}_k^H\mathbf{s}_k|^2}{p_u\sum_{i=1,i\neq k}^{K}|\mathbf{w}_k^H\mathbf{s}_i|^2+\parallel\mathbf{w}_k\parallel^2}\right)\right\} \ . \tag{3.9}$$

where $\mathbb{E}$ is the expectation.

Eqn.(3.9) is a lower capacity bound where data transmission is encoded for different realizations from the sources of randomness which enter the model from both the channel and noise. The uplink sum rate per cell is given as

$$C_P = \sum_{k=1}^{K} R_{P,k} \ . \tag{3.10}$$

With the BS having a perfect CSI, user transmit power can be scaled with M according to $p_u = \frac{E_u}{M}$ if needed, where E_u is held constant. Using the MRC from Eqn.(3.6), $\mathbf{w}_k = \mathbf{s}_k$ the achievable uplink rate in Eqn.(3.9) of the kth user can be written as

$$R_{P,k}^{mrc} = \mathbb{E}\left\{\log_2\left(1+\frac{p_u\parallel\mathbf{s}_k\parallel^4}{p_u\sum_{i=1,i\neq k}^{K}|\mathbf{s}_k^H\mathbf{s}_i|^2+\parallel\mathbf{s}_k\parallel^2}\right)\right\} \ , \tag{3.11}$$

Using the convexity of $\log_2\left(1+\frac{1}{x}\right)$ in Eqn.(3.11) and applying Jensen's inequality i.e., $(\mathbb{E}[Y] = \mathbb{E}[\rho(X)] \geq \rho(\mathbb{E}[(X)])$ [12][28], a lower bound is derived for the

achievable rate in Eqn.(3.11),

$$R_{P,k}^{mrc} \geq \tilde{R}_{P,k}^{mrc} \triangleq \log_2 \left(1 + \left(\mathbb{E} \left\{ \frac{p_u \sum\limits_{i=1, i \neq k}^{K} |\mathbf{s}_k^H \mathbf{s}_i|^2 + \| \mathbf{s}_k \|^2}{p_u \| \mathbf{s}_k \|^4} \right\} \right)^{-1} \right) . \quad (3.12)$$

3.2.2 Capacity Analysis for MRC Receivers

The analysis of the SINR for MRC receivers in large-scale MIMO is derived in this subsection. Using the inner terms of Eqn.(3.12) i.e.,

$$\mathbb{E} \left\{ \frac{p_u \sum\limits_{i=1, i \neq k}^{K} |\mathbf{s}_k^H \mathbf{s}_i|^2 + \| \mathbf{s}_k \|^2}{p_u \| \mathbf{s}_k \|^4} \right\}, \quad (3.13)$$

we can rewrite the above equation by taking common term of the denominator $\| \mathbf{s}_k \|^2$ to have

$$\mathbb{E} \left\{ \left(\frac{p_u \sum\limits_{i=1, i \neq k}^{K} |\mathbf{s}_k^H \mathbf{s}_i|^2}{\| \mathbf{s}_k \|^2} + 1 \right) \left(\frac{1}{p_u \| \mathbf{s}_k \|^2} \right) \right\}, \quad (3.14)$$

for the first term in Eqn.(3.14) i.e.,

$$\left(\frac{p_u \sum\limits_{i=1, i \neq k}^{K} |\mathbf{s}_k^H \mathbf{s}_i|^2}{\| \mathbf{s}_k \|^2} + 1 \right), \quad (3.15)$$

by dealing with the numerator and denominators without the summation and power notations we have

$$\frac{|\mathbf{s}_k^H \mathbf{s}_i|^2}{\| \mathbf{s}_k \|^2}, \tag{3.16}$$

therefore we can define a R.V. $\tilde{s}_i$ where

$$\tilde{s}_i \triangleq \frac{\mathbf{s}_k^H \mathbf{s}_i}{\| \mathbf{s}_k \|}, \tag{3.17}$$

where $\tilde{s}_i$ is independent of $\mathbf{s}_k$ [53]. The mean and variance of the R.V. $\tilde{s}_i$ conditioned on $\mathbf{s}_k$ are respectively [53],

$$\mathbb{E}[\tilde{s}_i|\mathbf{s}_k] = \frac{\mathbf{s}_k^H}{|\mathbf{s}_k|}\mathbb{E}[\mathbf{s}_i], \tag{3.18}$$

and

$$\mathbb{E}[|\tilde{s}_i|^2|\mathbf{s}_k] = \frac{\mathbf{s}_k^H \mathbb{E}[\mathbf{s}_i \mathbf{s}_i^H]\mathbf{s}_k}{|\mathbf{s}_k|^2}, \tag{3.19}$$

The above expressions hold for an arbitrary number of antennas and interference sources. By using the results obtained in Eqn.(3.17) $\tilde{s}_i$, Eqn.(3.14) reduces to

$$\left(p_u \sum_{i=1, i\neq k}^{K} \mathbb{E}\{|\tilde{s}_i|^2\} + 1 \right) \mathbb{E}\left\{ \frac{1}{p_u \| \mathbf{s}_k \|^2} \right\} \tag{3.20}$$

In the next section different fading scenarios that occur in literature are discussed and new tractable formulas for ergodic capacity are derived by using the above analysis in this section.

3.2.3 Rician Fading with Independent Rayleigh Interferers

In this model, a desired kth user undergoes Rician fading and is also affected by interference with Rayleigh distribution. By setting $s_{mk} = h_{mk}\sqrt{\gamma_k}$ using Eqn.(3.19), $\mathbb{E}\{|\tilde{s}_i|^2\}$ is evaluated in Eqn.(3.20). For analytical tractability, a set of complex-valued vectors are defined for the analysis, for users

$$\mathbf{S}_k = \begin{bmatrix} h_{1,k}\sqrt{\gamma_k} \\ \vdots \\ h_{m,k}\sqrt{\gamma_k} \end{bmatrix}, \quad \mathbf{S}_k^H = \begin{bmatrix} h_{1,k}^H\sqrt{\gamma_k} & \cdots & h_{m,k}^H\sqrt{\gamma_k} \end{bmatrix} \quad m = 1, 2, ..., M, \;\; k = 1, 2, ..., K. \tag{3.21}$$

for the interferers we have

$$\mathbf{S}_i = \begin{bmatrix} h_{1,i}\sqrt{\gamma_i} \\ \vdots \\ h_{m,i}\sqrt{\gamma_i} \end{bmatrix}, \quad \mathbf{S}_i^H = \begin{bmatrix} h_{1,i}^H\sqrt{\gamma_i} & \cdots & h_{m,i}^H\sqrt{\gamma_i} \end{bmatrix} \quad m = 1, 2, ..., M, \;\; i = 1, 2, ..., I. \tag{3.22}$$

Proposition 1: Under Rician fading and perfect CSI with $M \geq 2$, a lower bound on the ergodic uplink achievable rate from the kth user using the MRC is derived by substituting Eqn.(A.22) in Eqn.(3.12),

$$\tilde{R}_{P,k}^{mrc} = \log_2 \left(1 + \frac{2p_u(M-1)\gamma_k}{(p_u \sum\limits_{i=1, i\neq k}^{K} \gamma_i + 1)({}_1F_1\left(M-1, M; K_r M\right) e^{-K_r M})} \right). \tag{3.23}$$

where ${}_1F_1$ is the Kummer's confluent Hypergeometric function.

Proof: The proof is derived in Appendix A.

Remark 1: when K_r= 0 it matches perfectly to that in [12] as Rayleigh fading with $\gamma_k = \frac{1}{2}$.

Proposition 2: Under Rician fading and perfect CSI with $M \geq 2$, a lower bound on the ergodic uplink asymptotic rate is derived as

$$\tilde{R}_{P,k}^{mrc} = \log_2 \left(1 + \frac{2Mp_u(1+K_r)(2M+2K_rM)^3\gamma_k}{(p_u \sum_{i=1,i\neq k}^{K} \gamma_i + 1)(8M(1+K_r)(M+2K_rM) + (2M+2K_rM)^3)} \right), \tag{3.24}$$

Proof: The proof is derived in Appendix A.

Remark 2: If only the first term in Eqn.(A.17) is used in Eqn.(3.24), therefore we have

$$\tilde{R}_{P,k}^{mrc} = \log_2 \left(1 + \frac{2Mp_u(1+K_r)\gamma_k}{(p_u \sum_{i=1,i\neq k}^{K} \gamma_i + 1)} \right). \tag{3.25}$$

3.2.4 Rician Fading with Independent Rician Interferers

In the case of Rician interferers the fast fading coefficients $h_{m,i}$ are i.i.d complex-valued random variables with densities $h_{m,i} \sim \mathcal{CN}$ ($\sqrt{K_i}$,1) and $|h_{m,i}|^2$ follows a noncentral chi-square distribution.

Using Theorem 1.4.5 in [54] and the corollary A of [53], a $2M$ dimensional random

vector $\mathbf{v}$ is defined as

$$\mathbf{v} = \begin{bmatrix} h_{1,i} \\ \vdots \\ h_{m,i} \end{bmatrix}, \tag{3.26}$$

where

$$\mathbb{E}[\mathbf{v}] = \sqrt{K_i} \begin{bmatrix} 1 \\ \vdots \\ 1 \end{bmatrix} \quad \text{and} \quad \mathbb{E}[(\mathbf{v} - \mathbb{E}[\mathbf{v}])(\mathbf{v} - \mathbb{E}[\mathbf{v}])^T] = (1/2)\mathbf{I}_{2M} \tag{3.27}$$

by setting $\mathbf{s} \triangleq \sqrt{2}\ \mathbf{v}$, $\mathbf{s}$ meets the conditions in the corollary A of [53].

For the analysis in this section a new set of complex-valued vectors are defined using Eqn.(3.26), for users

$$\mathbf{S}_k = \sqrt{2} \begin{bmatrix} h_{1,k}\sqrt{\gamma_k} \\ \vdots \\ h_{m,k}\sqrt{\gamma_k} \end{bmatrix}, \quad \mathbf{S}_k^H = \sqrt{2} \begin{bmatrix} h_{1,k}^H\sqrt{\gamma_k} & \cdots & h_{m,k}^H\sqrt{\gamma_k} \end{bmatrix} \ \ 1 \le k \le K, \ \ 1 \le m \le M. \tag{3.28}$$

and for interferers

$$\mathbf{S}_i = \sqrt{2} \begin{bmatrix} h_{1,i}\sqrt{\gamma_i} \\ \vdots \\ h_{m,i}\sqrt{\gamma_i} \end{bmatrix}, \quad \mathbf{S}_i^H = \sqrt{2} \begin{bmatrix} h_{1,i}^H\sqrt{\gamma_i} & \cdots & h_{m,i}^H\sqrt{\gamma_i} \end{bmatrix} \ \ 1 \le i \le I, \ \ 1 \le m \le M. \tag{3.29}$$

From Eqn.(3.20), evaluating $\mathbb{E}\{|\tilde{s}_i|^2\}$ using the new set of vectors we have

$$\mathbb{E}\{|\tilde{s}_i|^2\} = \frac{\sqrt{2}\begin{bmatrix} h_{1,k}^H\sqrt{\gamma_k} & h_{2,k}^H\sqrt{\gamma_k}\end{bmatrix}\mathbb{E}\left[\sqrt{2}\begin{bmatrix} h_{1,i}\sqrt{\gamma_i} \\ h_{2,i}\sqrt{\gamma_i}\end{bmatrix}\sqrt{2}\begin{bmatrix} h_{1,i}^H\sqrt{\gamma_i} & h_{2,i}^H\sqrt{\gamma_i}\end{bmatrix}\right]\sqrt{2}\begin{bmatrix} h_{1,k}\sqrt{\gamma_k} \\ h_{2,k}\sqrt{\gamma_k}\end{bmatrix}}{\left[\sqrt{2}\begin{bmatrix} h_{1,k}^H\sqrt{\gamma_k} & h_{2,k}^H\sqrt{\gamma_k}\end{bmatrix}\sqrt{2}\begin{bmatrix} h_{1,k}\sqrt{\gamma_k} \\ h_{2,k}\sqrt{\gamma_k}\end{bmatrix}\right]} \tag{3.30}$$

by evaluating the inner terms of the numerator in Eqn.(3.30), we have

$$\mathbb{E}[\mathbf{s}_i\mathbf{s}_i^H] = 2\left\{\mathbb{E}\begin{bmatrix} |h_{1,i}|^2\gamma_i & h_{1,i}h_{2,i}^H\gamma_i \\ h_{1,i}^Hh_{2,i}\gamma_i & |h_{2,i}|^2\gamma_i\end{bmatrix}\right\} \tag{3.31}$$

from Eqn.(3.27) and since $Var(h) = \mathbb{E}[|h|^2] - (\mathbb{E}[h])^2$ with $Var(h) = 1/2$ and $(\mathbb{E}[h])^2 = K_i$, where K_i is the interference Rice factor then $\mathbb{E}[|h|^2] = K_i + 1/2$ and due to independence i.e., $(\mathbb{E}[h_{1,i}h_{2,i}^H] = \mathbb{E}[h_{1,i}^Hh_{2,i}] = 0)$, Eqn.(3.31) reduces to

$$\mathbb{E}[\mathbf{s}_i\mathbf{s}_i^H] = 2(K_i + 1/2)\gamma_i\begin{bmatrix} 1 & 0 \\ 0 & 1\end{bmatrix}, \tag{3.32}$$

then,

$$\mathbf{s}_k^H\mathbb{E}[\mathbf{s}_i\mathbf{s}_i^H]\mathbf{s}_k = \sqrt{2}\begin{bmatrix} h_{1,k}^H\sqrt{\gamma_k} & h_{2,k}^H\sqrt{\gamma_k}\end{bmatrix}.2(K_i + 1/2)\gamma_i\begin{bmatrix} 1 & 0 \\ 0 & 1\end{bmatrix}\sqrt{2}\begin{bmatrix} h_{1,k}\sqrt{\gamma_k} \\ h_{2,k}\sqrt{\gamma_k}\end{bmatrix}. \tag{3.33}$$

Evaluating Eqn.(3.33) from left to right , the equation reduces to

$$\mathbf{s}_k^H \mathbb{E}[\mathbf{s}_i \mathbf{s}_i^H] \mathbf{s}_k = 4(K_i + 1/2)\gamma_i \gamma_k \left[|h_{1,k}|^2 + |h_{2,k}|^2 \right]. \tag{3.34}$$

The denominator in Eqn.(3.30) is evaluated as

$$\sqrt{2} \begin{bmatrix} h_{1,k}^H \sqrt{\gamma_k} & h_{2,k}^H \sqrt{\gamma_k} \end{bmatrix} \sqrt{2} \begin{bmatrix} h_{1,k} \sqrt{\gamma_k} \\ h_{2,k} \sqrt{\gamma_k} \end{bmatrix} = 2\gamma_k \left[|h_{1,k}|^2 + |h_{2,k}|^2 \right], \tag{3.35}$$

combining the results of both Eqn.(3.34) and Eqn.(3.35) in Eqn.(3.30)

$$\begin{aligned} \mathbb{E}\{|\tilde{s}_i|^2\} &= \frac{4(K_i + 1/2)\gamma_i \gamma_k \left[|h_{1,k}|^2 + |h_{2,k}|^2 \right]}{2\gamma_k \left[|h_{1,k}|^2 + |h_{2,k}|^2 \right]} \\ &= 2(K_i + 1/2)\gamma_i \ . \end{aligned} \tag{3.36}$$

Remark 3: When $K_i = 0$ (No Rician Interference), $\mathbb{E}\{|\tilde{s}_i|^2\}$ in Eqn.(3.36) equates to that of Eqn.(A.10) (Rayleigh Interference).

Using the result of Eqn.(3.36) in Eqn.(A.22) a new proposition is obtained.

Proposition 3: Under Rician fading and perfect CSI with $M \geq 2$ and the presence of Rician interferers, the uplink achievable rate from the kth user using MRC is,

$$\tilde{R}_{P,k}^{mrc} = \log_2 \left(1 + \frac{2p_u (M-1)\gamma_k}{(2p_u \sum_{i=1, i \neq k}^{K} (K_i + 1/2)\gamma_i + 1)({}_1F_1 \left(M-1, M; K_r M \right) e^{-K_r M})} \right), \tag{3.37}$$

Proof: The proof is derived using Appendix A.

Using the asymptotic expression in Eqn.(3.25), another proposition is stated.

Proposition 4: By using asymptotic equations in Eqn.(A.19) under Rican fading and perfect CSI with $M \geq 2$, in the presence of Rician interferers the uplink achievable rate from the kth user using MRC is

$$\tilde{R}_{P,k}^{mrc} = \log_2 \left(1 + \frac{2Mp_u(1+K_r)\gamma_k}{(2p_u \sum_{i=1, i\neq k}^{K} (K_i + 1/2)\gamma_i + 1)} \right) . \tag{3.38}$$

Proof: The proof is derived using Appendix A.

3.3 Capacity Analysis for Zero Forcing Receivers

The analysis for Zero-Forcing (ZF) receivers with perfect CSI is slightly different from that of MRC receivers. Using ZF receivers [18],

$$\mathbf{W}^H = (\mathbf{S}^H\mathbf{S})^{-1}\mathbf{S}^H, \tag{3.39}$$

which can be reduced to have

$$\mathbf{W}^H\mathbf{S} = \mathbf{I}_K. \tag{3.40}$$

Using Eqn.(3.40), the vector elements in Eqn.(3.9) can be written as $\mathbf{w}_k^H\mathbf{s}_i = \nu_{ki}$, where ν_{ki}= 1 for $k = i$ and $\nu_{ki} = 0$, otherwise. Using this notation in Eqn.(3.9),

therefore Eqn.(3.11) becomes

$$R_{P,k}^{zf} = \mathbb{E}\left\{\log_2\left(1 + \frac{p_u}{\left[(\mathbf{S}^H\mathbf{S})^{-1}\right]_{kk}}\right)\right\} \quad , \tag{3.41}$$

where $\left[(\mathbf{S}^H\mathbf{S})^{-1}\right]_{kk}$ denotes the $(k,k)^{th}$ (diagonal) elements of $(\mathbf{S}^H\mathbf{S})^{-1}$.

By making use of Jensen's inequality as previously stated in Sec.(3.2.1) in Eqn.(3.41), a lower bound using ZF receivers on the achievable rate is

$$R_{P,k}^{zf} \geq \tilde{R}_{P,k}^{zf} = \log_2\left(1 + \frac{p_u}{\mathbb{E}\left\{\left[(\mathbf{S}^H\mathbf{S})^{-1}\right]_{kk}\right\}}\right) \quad . \tag{3.42}$$

3.3.1 ZF receivers in Rician Fading with Independent Rayleigh Interferers

For the kth user in Rician fading channels with ZF receivers, the denominator in Eqn.(3.42), i.e., $\mathbf{S}^H\mathbf{S}$ follows a complex non-central Wishart distribution, which is denoted by $\mathbf{S}^H\mathbf{S} \backsim \mathcal{W}_K(p, \mathbf{\Sigma}, \Theta)$ [55], where p represents the degrees of freedom, Σ is the covariance matrix and Θ is the noncentrality matrix.

From [56], the n-th inverse moment of the determinant of a complex non-central Wishart distribution is defined as

$$\mathbb{E}\{|\mathbf{A}|^{-n}\} = {}_1F_1\left(\frac{p}{2} - n, \frac{p}{2}; \Theta\right) \frac{e^{-tr(\Theta)}}{2^{kn}} \frac{\Gamma_k(\frac{p}{2} - n)}{\Gamma_k(\frac{p}{2})} \quad , \tag{3.43}$$

where $\mathbf{A}$ follows a non-central complex Wishart distribution, ${}_1F_1$ is the confluent hypergeometric function and Γ_k is the multivariate gamma function [57]. By setting the values for $n = 1$, $p = 2M$, $tr(\Theta) = 2K_rM$, therefore, Eqn.(3.43) reduces to

$$\mathbb{E}\{|A|^{-1}\} =_1 F_1\left(M-1, M; 2K_rM\right) \frac{e^{-2K_rM}}{2^k} \frac{\Gamma_k(M-1)}{\Gamma_k(M)} \quad . \tag{3.44}$$

Remark 4: When $(\Theta) = 0$ (i.e., $K_r = 0$) the non-central Wishart distribution reduces to the central Wishart matrix used in [12]. Since the SNR distribution of each stream is the same the subscript k in $\left[(\mathbf{S}^H\mathbf{S})^{-1}\right]_{kk}$ can be dropped [58].

Proposition 5: Using ZF receivers in Rician fading channels with $M \geq 2$ (i.e., by replacing Eqn.(3.44) in Eqn.(3.42)), a lower bound for the achievable uplink rate from the desired user is

$$\tilde{R}_{P,k}^{zf} = \log_2\left(1 + \frac{2^k p_u \gamma_k \Gamma_k(M)}{{}_1F_1\left(M-1, M; 2K_rM\right) e^{-2K_rM}\Gamma_k(M-1)}\right) \quad . \tag{3.45}$$

3.4 Results and Discussions

Fig. 3.2 shows the exact plots against the asymptotic plots which shows that the asymptotic derivations work perfectly as the exact derivations when M grows large. Fig. 3.3 shows the plot when K_r is set to 0 ($-\infty$ dB) and it matches to the previous work in [12] as Rician fading equates to Rayleigh fading. The simulations in Fig. 3.3 shows the ergodic capacity based on Perfect CSI, the lower bound and the Monte Carlo simulations is carried out with $K_r = 0$ (this matches

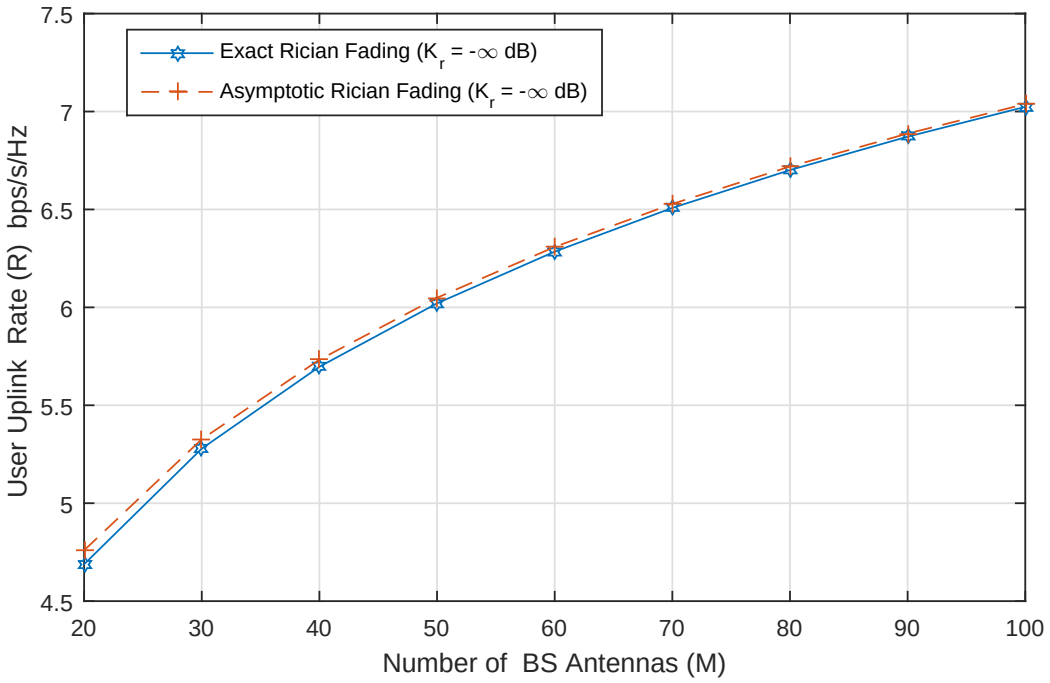

Figure 3.2: Comparison between exact and asymptotic plots under Rician fading $K_r = 0$ (-∞ dB) using MRC receivers with transmit power $p_u = 10$ dB.

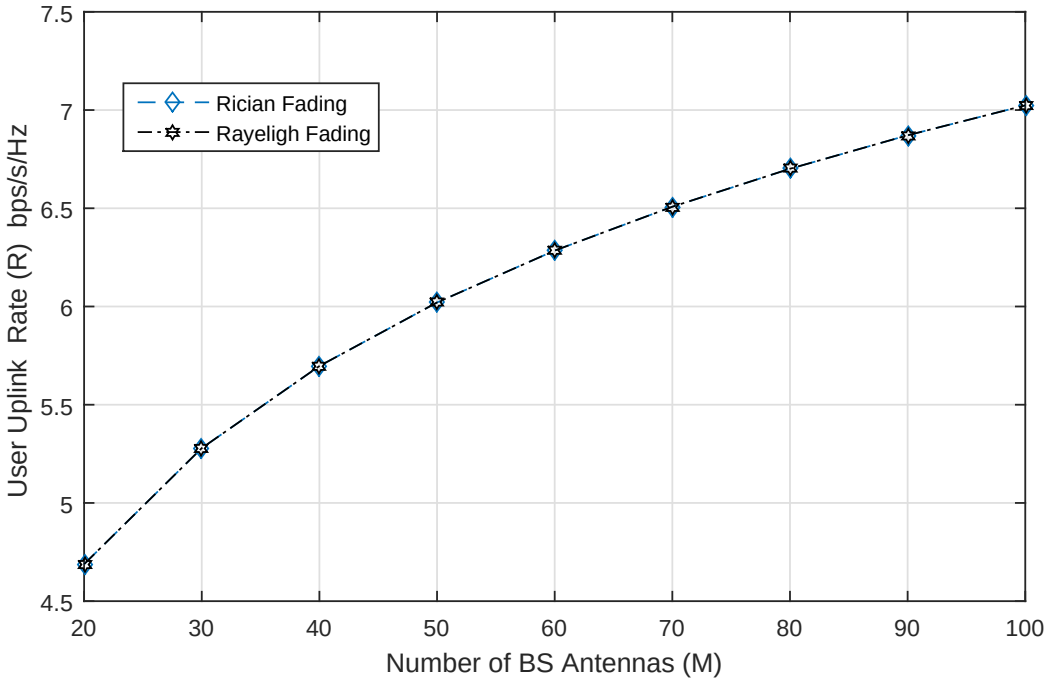

Figure 3.3: Ergodic Capacity matching between Rician and Rayleigh Fading with $K_r = 0$ (-∞ dB) using MRC receivers with transmit power $p_u = 10$ dB.

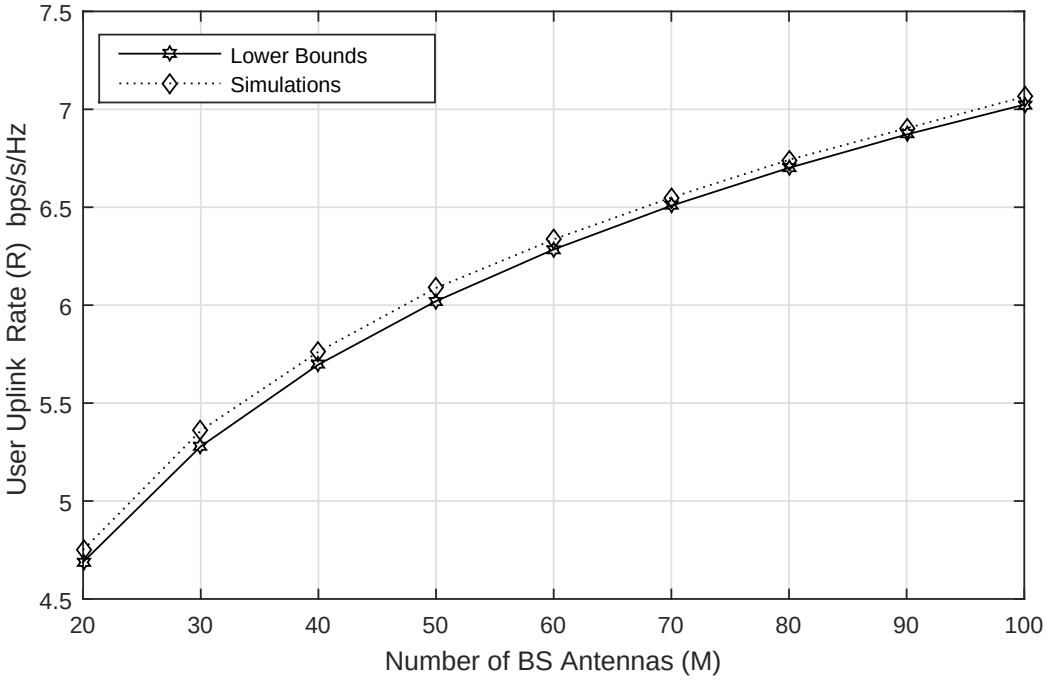

Figure 3.4: Ergodic Capacity under Rician Fading with Monte Carlo simulations $K_r = 0$ (-∞ dB) using MRC receivers with transmit power $p_u = 10$ dB.

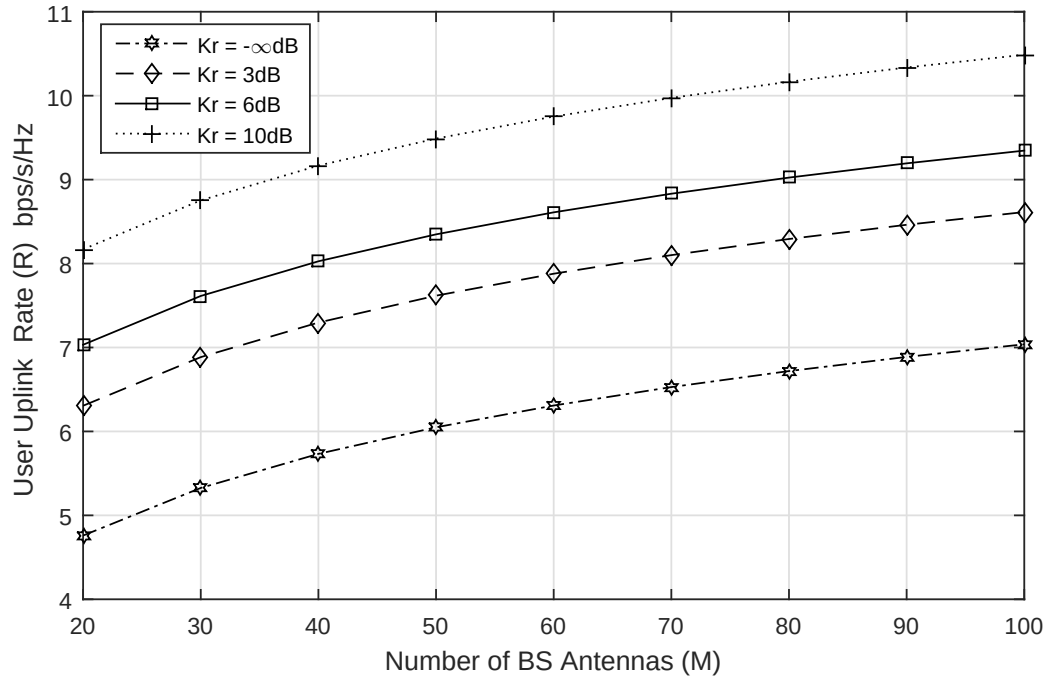

Figure 3.5: Ergodic Capacity under Rician Fading with increasing values of K_r using lower bounds of MRC receivers with transmit power $p_u = 10$ dB.

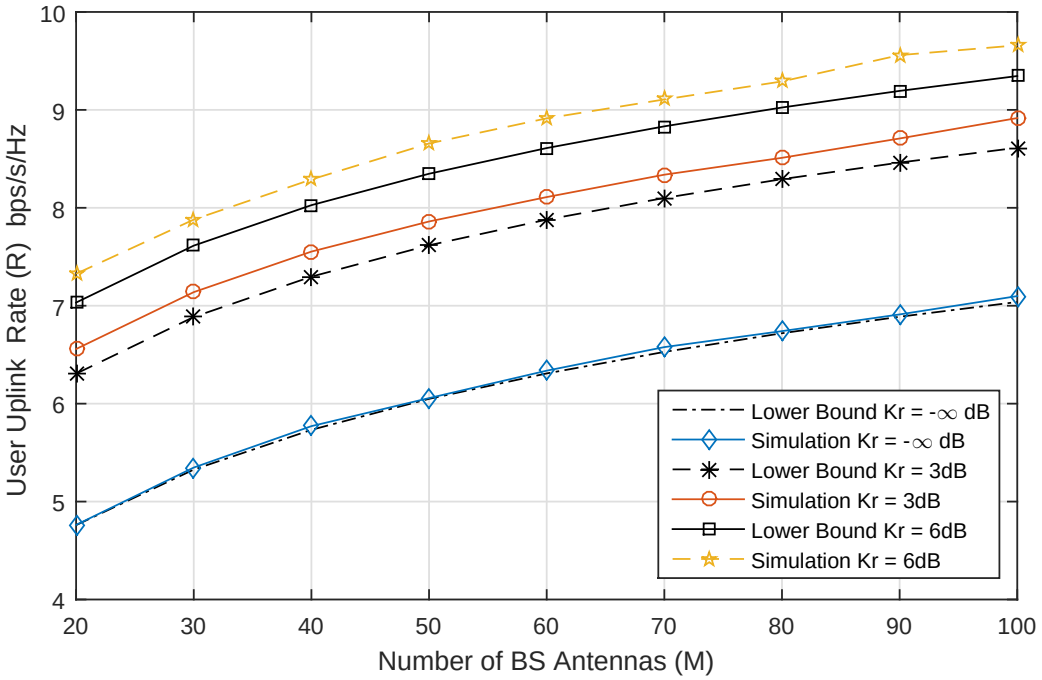

Figure 3.6: Ergodic Capacity under Rician Fading with Monte Carlo simulations with increasing values of K_r using MRC receivers with transmit power $p_u = 10$ dB.

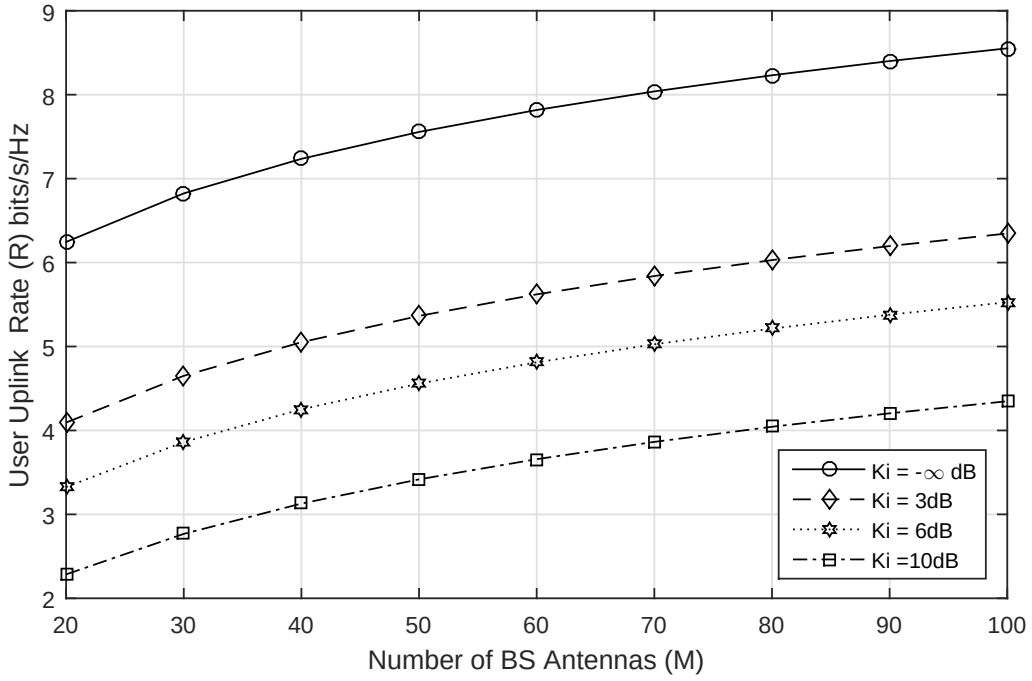

Figure 3.7: Ergodic Capacity under Rician Fading with Rician interference (K_r = 3dB) using lower bounds of MRC receivers with transmit power $p_u = 10$ dB.

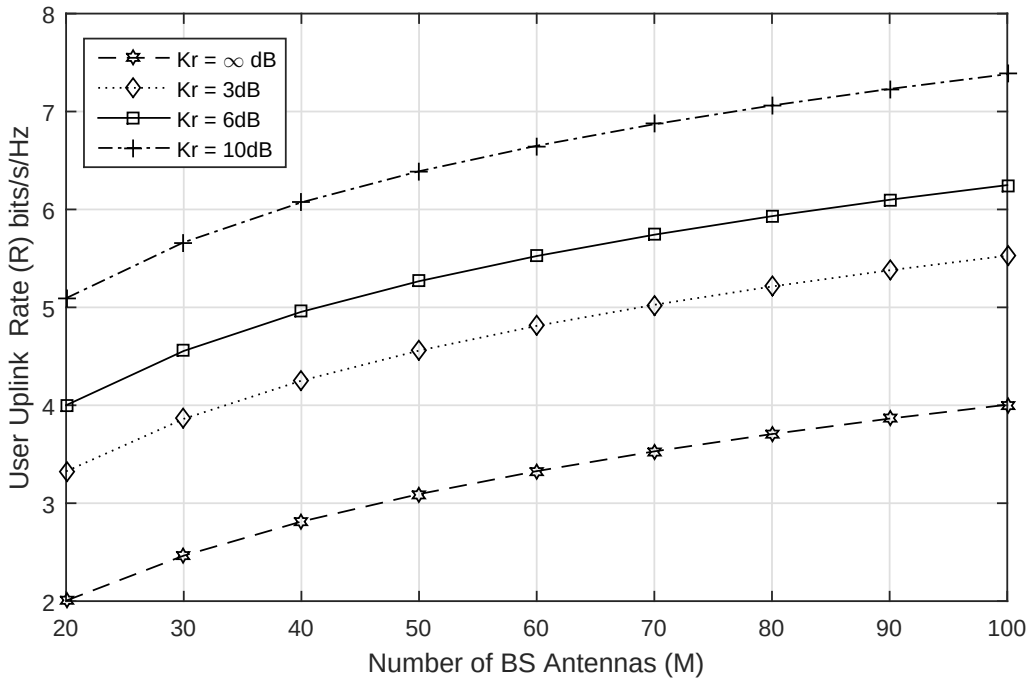

Figure 3.8: Ergodic Capacity under Rician Fading with Rician interference (K_i = 6dB) using lower bounds of MRC receivers with transmit power p_u = 10 dB.

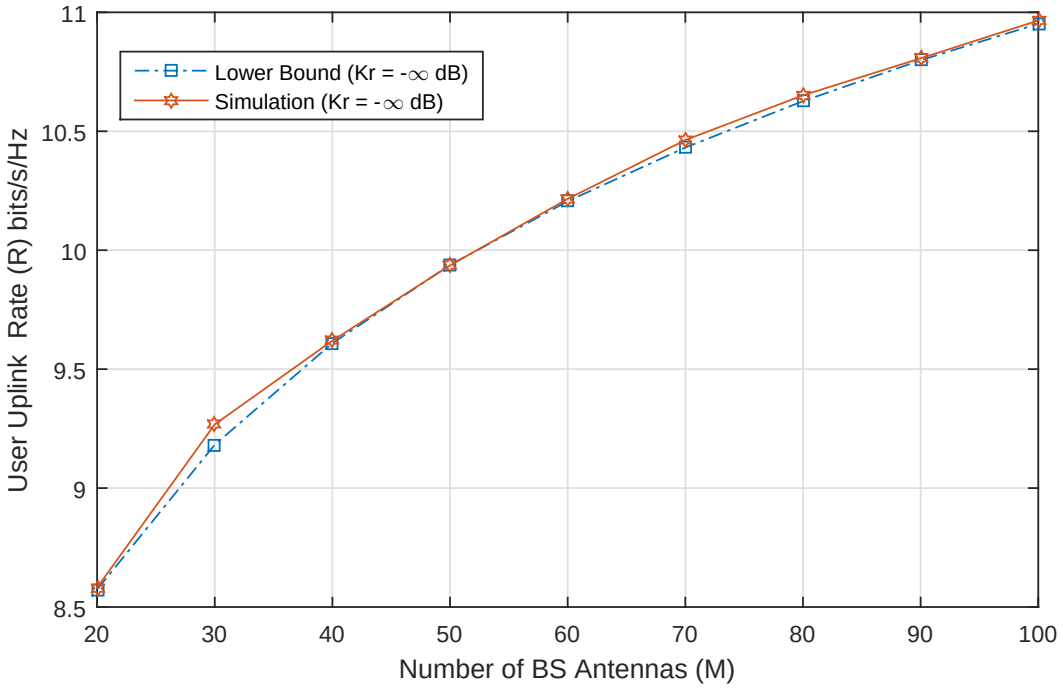

Figure 3.9: Ergodic Capacity under Rician Fading with Monte Carlo simulations $K_r = 0$ (-∞ dB) using ZF receivers with transmit power p_u = 10 dB.

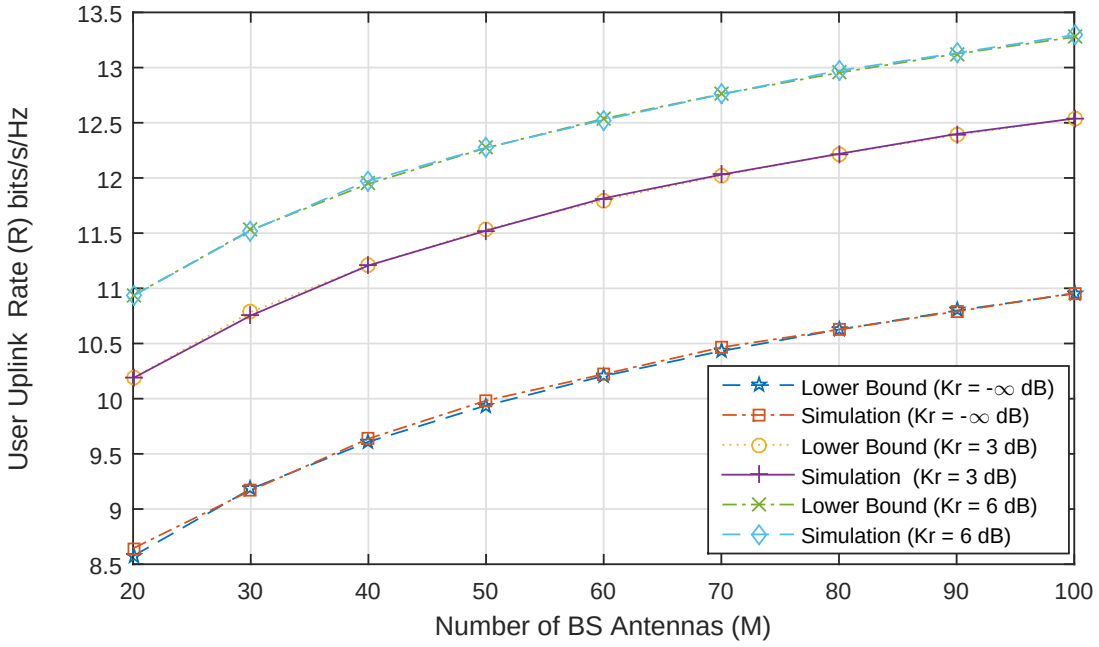

Figure 3.10: Ergodic Capacity under Rician Fading with increasing values of K_r with Monte Carlo simulations using ZF receivers with transmit power $p_u = 10$ dB.

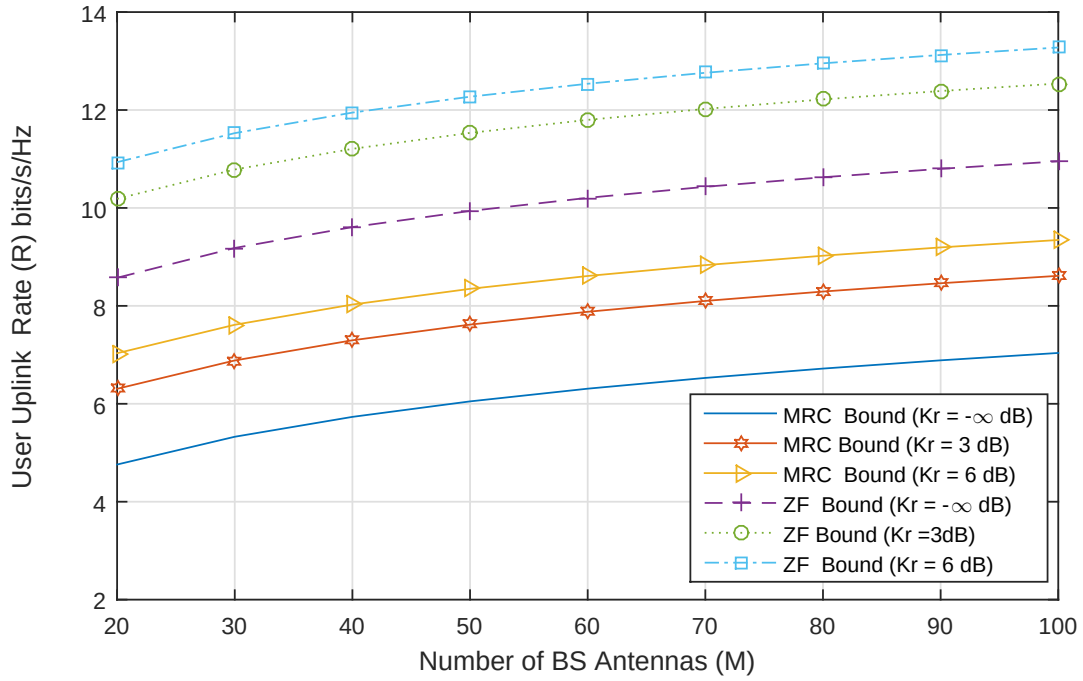

Figure 3.11: Comparison of Ergodic Capacity under Rician Fading with increasing values of K_r using both ZF and MRC receivers with transmit power $p_u = 10$ dB.

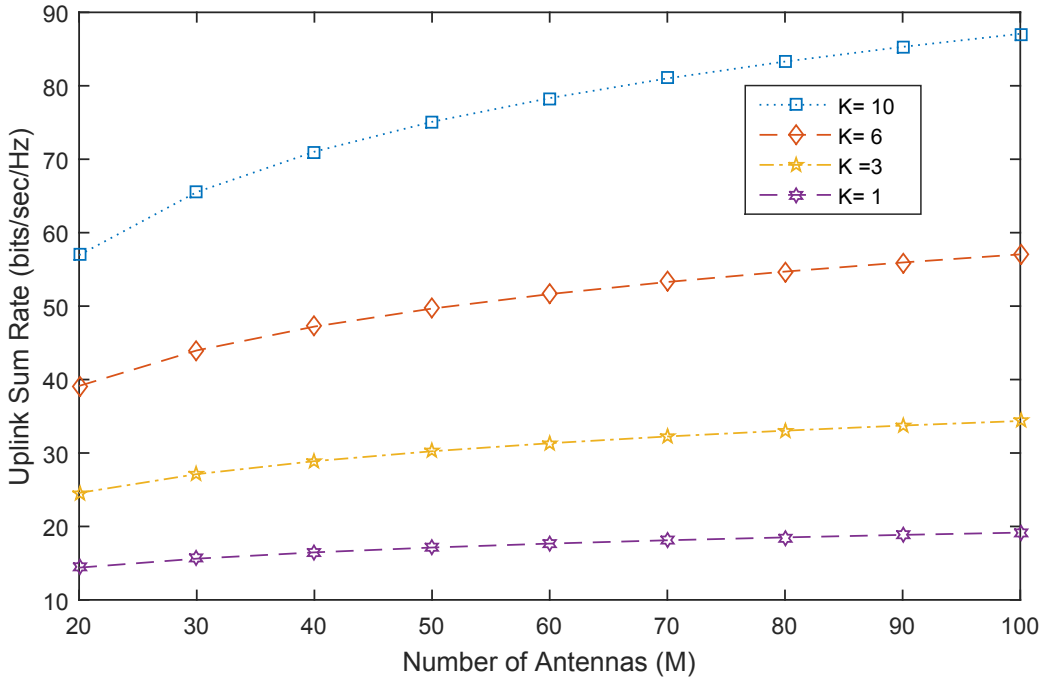

Figure 3.12: Ergodic Capacity under Rician Fading with increasing number of K-user antennas (K_r = 3dB) using ZF receivers.

to the Rayleigh scenario in [12]). With an increase in K_r ($-\infty$ dB to 10 dB) it can be seen that the desired user uplink rate increases (4.7 bits/s/Hz to 8.3 dB bits/s/Hz) as M increases as well from 20 to 100 antennas, where a large K_r indicates more mild fading scenario [23] and also as the number of base station antennas M increases the capacity of the desired user also improves as shown in Fig. 3.5 and Fig. 3.6.

Figure 3.6 also shows the Monte Carlo simulations with the analytical results of the lower bound capacity expressions that have been derived it can be seen that the simulation either matches (K_r = -∞ dB) or slightly above the bounds in the case of (K_r = 3 dB and 6 dB) this goes in agreement with the achievable rate equal to or greater that the lower bound derived (see Sec. 3.2.1). The plot in

Fig. 3.7 shows the effect of interference on capacity, with an increase in K_i of interferers the capacity of the desired user reduces ($K_r = 3$ dB is kept constant) and this shows the effect of multipath fading in respect to capacity. Fig. 3.8 shows when the fading effect on the desired user is reduced in the presence of interferers ($K_i = 10$ dB) by an increase in K_r of the desired user there is an improvement in capacity.

The simulation of Fig. 3.9 shows the performance of the ZF receiver using Monte Carlo simulations matching with the lower bounds derived ($K_r = -\infty$ dB), it can be observed that the capacity for the desired user is increased using the ZF receiver with perfect CSI, due to its ability to negate inter-user interference the ZF gives a better performance than the MRC from the simulations with the same increase of K_r under Rician fading (see Figure 3.11).

Fig. 3.10 shows Monte Carlo simulations using the ZF receiver for a desired user uplink rate matching with the lower bounds derived as the Rician factor ($K_r = -\infty$ dB, 3 dB and 6 dB) increases, and improvement of the desired user uplink rate is seen to increase from 8 bits /s/Hz to 11 bits/s/Hz with an increase in M antennas from 20 to 100 antennas.

The improvement in capacity using large-scale MIMO can be seen with an increase in K single-antenna users, higher rates is achieved as the BS transmits data among different users using identical time-frequency resources as shown using the ZF receiver in Fig. 3.12, as the number of users increase the uplink sum rate capacity (12 bits/s/Hz to 58 bits/s/Hz) with an increase in M antennas from 20 to 100

antennas increases tremendously which shows the viability of large-scale MIMO [36]. The computational complexity (Multivariate Gamma function) is added using the ZF receiver as when compared to the MRC receiver.

CHAPTER 4

CAPACITY OF LARGE-SCALE MIMO OVER SHADOWED FADING CHANNELS

4.1 Composite Fading Models

In general, large-scale MIMO channels undergo both small and large scale fading (due to large antenna arrays) [10]. Small scale fading is caused by local scatterers around receivers and large scale fading is caused by reflection, scattering and diffraction due to large scatterers, i.e., terrain, vegetation just to name a few. Small scale fading is known as multi-path fading and large scale fading results in shadowing and when these phenomena occur simultaneously, it is called composite fading.

Small-scale multipath fading is usually modeled using either Rayleigh, Rician

or Nakagami distributions in literature [59] and large-scale fading (shadowing) is often modeled using the log-normal distribution. Different composite fading models have being proposed in literature for both line-of-sight (LOS) and non line-of-sight (NLOS) multipath fading as highlighted by the Table 4.1 below [60].

Table 4.1: Proposed composite fading models in wireless RF channels

Model	**Multipath**	**Shadowing**	**Summary**
Rayeleigh-lognormal	Rayleigh	lognormal	Best Fit for NLOS channels but not tractable.
Rician-lognormal	Rician	lognormal	Best Fit for LOS channels but intractable
Nakagami-lognormal	Nakagami	lognormal	Best Fit for both NLOS and LOS channels but intractable.
K-distribution	Rayleigh	gamma	Limitation to NLOS channels only but tractable.
Gamma-Gamma	Nakagami	gamma	A good fit for both LOS and NLOS channels and also tractable.
Weibull-gamma	Weibull	gamma	Currently no empirical validation and not as tractable as the gamma-gamma model.
Nakagami-Inverse Gaussian	Nakagami	Inverse Gaussian	Provides a good fit to lognormal-based models but its less tractable than the gamma-gamma model.
Beckmann-lognormal	Beckmann	lognormal	A generic scattering model but not tractable.
η - μ gamma	η - μ	gamma	Flexible model but its less tractable than the gamma-gamma model.

In reference to the Table 4.1 above the gamma-gamma composite fading model

would be used in this section since it provides tractability and also provides a good fit for both NLOS (Rayleigh) and LOS (Rician) multipath fading. In the previous chapter the shadowing parameter γ_k was held constant, but in this chapter the parameter γ_k is assumed to be a random variable.

4.2 The Gamma-Gamma Composite Fading Model

When the random variation of the envelope of the received signal, due to small-scale multipath fading, is modeled by a Nakagami distribution [60], the PDF of the received power γ, conditioned on the average local power Ω, takes the form of a Gamma distribution:

$$p_{\gamma/\Omega}(x) = \frac{1}{\Gamma(m_m)} \left(\frac{m_m}{\Omega}\right)^{m_m} x^{m_m-1} \exp\left(-\frac{m_m x}{\Omega}\right), \; x > 0, m_m \geq 0.5, \qquad (4.1)$$

where $\Gamma(\cdot)$ is the Gamma function and m_m is the Nakagami multipath fading parameter.

The variation of the average local power, due to shadowing, is usually modeled by the lognormal distribution [30]. However, the analytically better tractable Gamma distribution has also shown a good fit to data obtained through propagation measurements [61][62]. It is used to approximate the lognormal distribution

for the relevant range of shadowing severity in wireless channels (see Sec. 2.3.3).

The relationship between the parameters of the gamma model and lognormal model (in Sec. 2.3.3) is derived as [30],

$$m_s = \frac{1}{e^{(\frac{\sigma_s}{8.686})^2} - 1} \ , \tag{4.2}$$

$$\Omega_s = P_r \sqrt{(m_s + 1)/m_s} \ , \tag{4.3}$$

m_s is the shadowing parameter, Ω_s is the local average power, σ_s standard deviation of the lognormal model. The standard deviation expressed in dB (shadowing spread or 'dB-spread') is denoted as σ_{dB}= 8.686σ_s [30] and P_r is the constant area mean power.

Adopting the gamma shadowing model and using the combination of both Eqn.(2.7) and Eqn.(4.1), the gamma-gamma PDF is derived as [60],

$$\begin{aligned} f_\gamma(x) =& \frac{2}{\Gamma(m_s)\Gamma(m_m)} \Xi^{m_s+m_m} x^{(\frac{m_s+m_m}{2})-1} \\ & \times K_{(m_s-m_m)}(2\Xi\sqrt{x}), \ x > 0, m_m \geq 0.5, m_s > 0, \end{aligned} \tag{4.4}$$

where $K_{(m_s-m_m)}(\cdot)$ is the modified Bessel function of the second kind and order $(m_s - m_m)$ and $\Xi = \sqrt{\frac{m_m m_s}{\Omega_0}}$.

4.3 Achievable Rates for Composite Fading Channels

4.3.1 Capacity Bounds for Independent Multipath Fading and Shadowing

The shadowing component, i.e., γ_k, is usually modeled with a lognormal distribution but due to issues with tractability using the lognormal distribution, an approximation to the gamma distribution has been proposed in reported literature [30][59] and this was stated in Chapter 2.

For the analysis, each element in the channel matrix $\mathbf{S}$ will follow a gamma-gamma distribution hence,

$$\begin{aligned} \| \mathbf{s}_{km} \|^2 &= s_{k1}^2 + s_{k2}^2 + ... + s_{km}^2 \\ &= \gamma_{k1}|h_{k1}|^2 + \gamma_{k2}|h_{k2}|^2 + ... + \gamma_{km}|h_{km}|^2. \end{aligned} \tag{4.5}$$

When the elements in Eqn.(4.5) are i.i.d, the distribution is well approximated by another gamma-gamma model R.V. whose PDF is derived as [31][62],

$$f_s(s;\tilde{m}_s,\tilde{m}_m,\tilde{\Omega}) = \frac{2(\tilde{m}_s\tilde{m}_m)^{\frac{\tilde{m}_s+\tilde{m}_m}{2}} s^{\frac{\tilde{m}_s+\tilde{m}_m}{2}-1}}{\Gamma(\tilde{m}_s)\Gamma(\tilde{m}_m)\tilde{\Omega}^{\frac{\tilde{m}_s+\tilde{m}_m}{2}}} K_{(\tilde{m}_s-\tilde{m}_m)}\left[2s^{1/2}\sqrt{\tilde{m}_s\tilde{m}_m/\tilde{\Omega}}\right] \tag{4.6}$$

where $\tilde{m}_s \geqslant 0$ and $\tilde{m}_m \geqslant 0$ are the distribution shaping parameters, $K_{(\tilde{m}_s-\tilde{m}_m)}$ is the modified Bessel function of the second kind and order $(\tilde{m}_s - \tilde{m}_m)$ [29, 8.407/1].

The distribution shape parameters in Eqn.(4.6) are

$$\tilde{m}_s = M m_s + \varepsilon_s \tag{4.7}$$

$$\tilde{m}_m = M m_m \tag{4.8}$$

$$\tilde{\Omega} = M \Omega_s \ , \tag{4.9}$$

where ε_s is the adjustment parameter and can be expressed as [62],

$$\varepsilon_s(M, m_s, m_m) = (M-1)\frac{-0.127 - 0.95 m_s - 0.0058 m_m}{1 + 0.00124 m_s + 0.98 m_m} \ . \tag{4.10}$$

The desired user follows a gamma-gamma R.V. while the interferers follow a lognormal R.V., therefore for the interfering shadowing component γ_i in Eqn.(A.4) follows a standard lognormal distribution. Re-evaluating the terms in Eqn.(A.5) as,

$$\mathbb{E}[\mathbf{s}_i \mathbf{s}_i^H] = \begin{bmatrix} \mathbb{E}\left(|h_{1,i}|^2\right)\mathbb{E}\left(\gamma_i\right) & 0 \\ 0 & \mathbb{E}\left(|h_{2,i}|^2\right)\mathbb{E}\left(\gamma_i\right) \end{bmatrix} \ , \tag{4.11}$$

which leads to

$$\begin{aligned} \mathbf{s}_k^H \mathbb{E}[\mathbf{s}_i \mathbf{s}_i^H] \mathbf{s}_k &= \begin{bmatrix} h_{1,k}^H \sqrt{\gamma_k}\{\mathbb{E}\left(|h_{1,i}|^2\right)\mathbb{E}\left(\gamma_i\right)\} & h_{2,k}^H \sqrt{\gamma_k}\{\mathbb{E}\left(|h_{2,i}|^2\right)\mathbb{E}\left(\gamma_i\right)\} \end{bmatrix} \begin{bmatrix} h_{1,k}\sqrt{\gamma_k} \\ h_{2,k}\sqrt{\gamma_k} \end{bmatrix} \\ &= |h_{1,k}|^2 \gamma_k \{\mathbb{E}\left(|h_{1,i}|^2\right)\mathbb{E}\left(\gamma_i\right)\} + |h_{2,k}|^2 \gamma_k \{\mathbb{E}\left(|h_{2,i}|^2\right)\mathbb{E}\left(\gamma_i\right)\} \, . \end{aligned} \tag{4.12}$$

By setting $\mathbb{E}\left(\gamma_i\right) = e^{0.5\sigma^2}$ for standard lognormal distribution [63] and with

$\mathbb{E}\left(|h_{1,i}|^2\right) = \mathbb{E}\left(|h_{2,i}|^2\right) = 1$, therefore Eqn.(A.10) reduces to

$$\mathbb{E}\{|\tilde{s}_i|^2\} = e^{0.5\sigma_i^2} \ . \tag{4.13}$$

Proposition 6: Under the gamma-gamma model and perfect CSI with $M \geq 2$ with independent shadowing for the desired user and lognormal shadowing for the interferers, the ergodic uplink achievable rate from the kth user using MRC can be obtained by substituting the expressions of Eqn.(4.13) and Eqn.(B.5) in Eqn.(3.12),

$$\tilde{R}_{P,k}^{mrc} = \log_2 \left(1 + \frac{p_u M \Omega_s \Gamma(Mm_m)\Gamma(Mm_s + \varepsilon_s)}{(p_u \sum\limits_{i=1, i\neq k}^{K} e^{0.5\sigma_i^2} + 1)((Mm_m)(Mm_s + \varepsilon_s)\Gamma(Mm_m - 1)\Gamma(Mm_s + \varepsilon_s - 1))} \right) . \tag{4.14}$$

Using the relation $\Gamma(n)$= (n-1)$\Gamma(n-1)$, the expression in Eqn.(4.14) is reduced to

$$\tilde{R}_{P,k}^{mrc} = \log_2 \left(1 + \frac{p_u M \Omega_s (Mm_m - 1)(Mm_s + \varepsilon_s - 1)}{(p_u \sum\limits_{i=1, i\neq k}^{K} e^{0.5\sigma_i^2} + 1)(Mm_m)(Mm_s + \varepsilon_s)} \right) . \tag{4.15}$$

Proof: The proof is derived in Appendix B.

4.3.2 Capacity Bounds for Independent Multipath Fading and Fully Correlated Shadowing

In the case of fully correlated shadowing the antenna array elements at the BS undergoes fully correlated shadowing, although in general literature shadowing and multipath components are independent. This section deals with correlation among shadowing components that sometimes exists in some physical scenarios when the receiving antennas or antenna ports are not sufficiently spaced by at least tens of meters apart from one another in the array at the BS [60] [31].

So

$$\begin{aligned} \| \mathbf{s}_{km} \|^2 &= s_{k1}^2 + s_{k2}^2 + ... + s_{km}^2 \\ &= \gamma_k \left(|h_{k1}|^2 + |h_{k2}|^2 + ... + |h_{km}|^2 \right), \end{aligned} \tag{4.16}$$

therefore $\| \mathbf{s}_{km} \|^2$ becomes a sum of identically distributed and fully correlated gamma-gamma R.V's, with new parameters

$$\tilde{m}_s = m_s \tag{4.17}$$

$$\tilde{m}_m = M m_m \tag{4.18}$$

$$\tilde{\Omega} = M \Omega_s \ . \tag{4.19}$$

The multipath fading parameter is scaled by M, while the shadowing parameter remains the same, since fully correlated shadowing is experienced while the multipath (small-scale fading) components remain independent.

Using the derivations from the previous section and substituting the new values of the shaping parameters $\tilde{m}_s$, $\tilde{m}_m$ and $\tilde{\Omega}$ in Eqn.(4.15),

Proposition 7: Under the gamma-gamma model and perfect CSI with $M \geq 2$ with fully correlated shadowing for the desired user and lognormal shadowing for the interferers, the ergodic uplink achievable rate from the kth user using MRC is,

$$\tilde{R}_{P,k}^{mrc} = \log_2 \left(1 + \frac{p_u M \Omega_s (M m_m - 1)(m_s - 1)}{(p_u \sum_{i=1, i \neq k}^{K} e^{0.5\sigma_i^2} + 1)(M m_m)(m_s)} \right) . \tag{4.20}$$

4.4 Results and Discussions

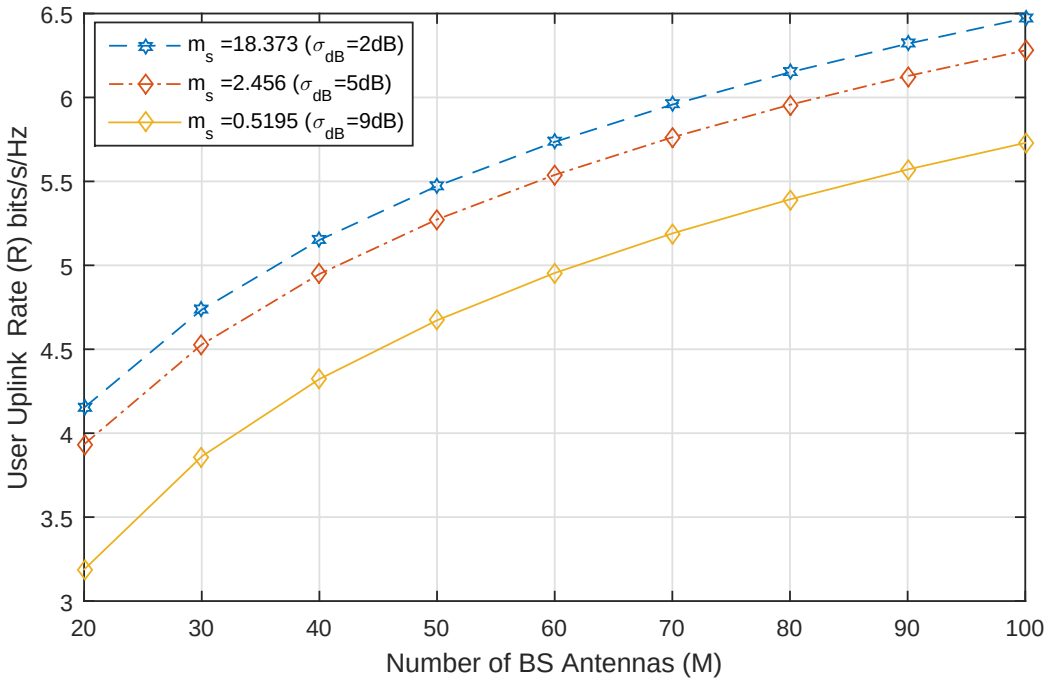

Figure 4.1: Ergodic Capacity under Rayleigh Fading with Independent Shadowing using MRC receivers ($m_m = 1, \Omega_s = 1$) with transmit power $p_u = 10$ dB.

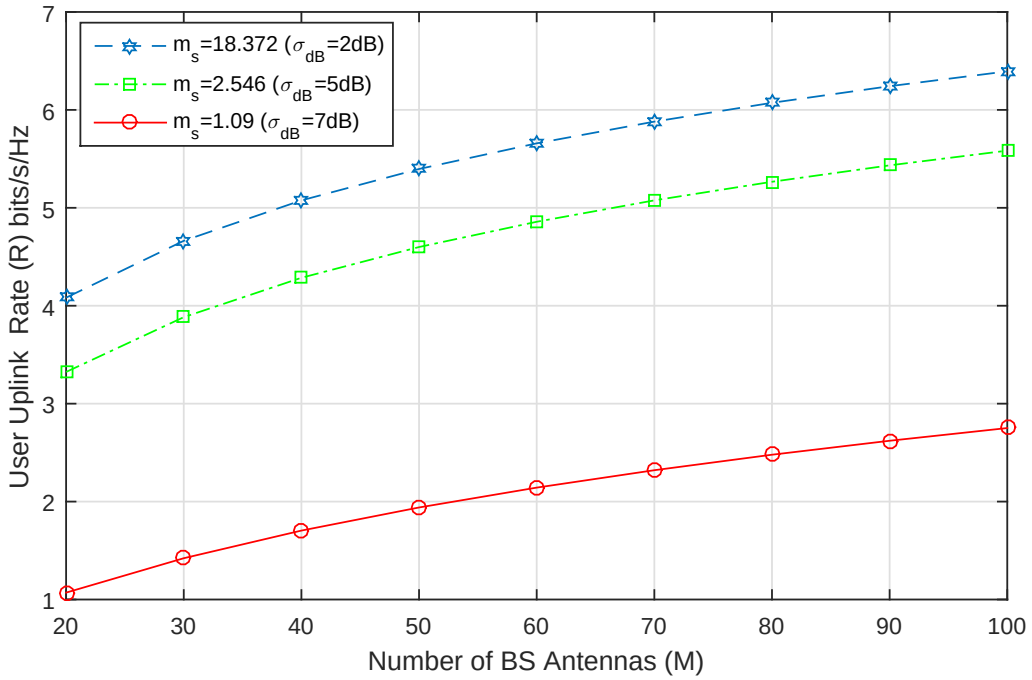

Figure 4.2: Ergodic Capacity under Rayleigh Fading with fully Correlated Shadowing using MRC receivers ($m_m = 1, \Omega_s = 1$) with transmit power $p_u = 10$ dB.

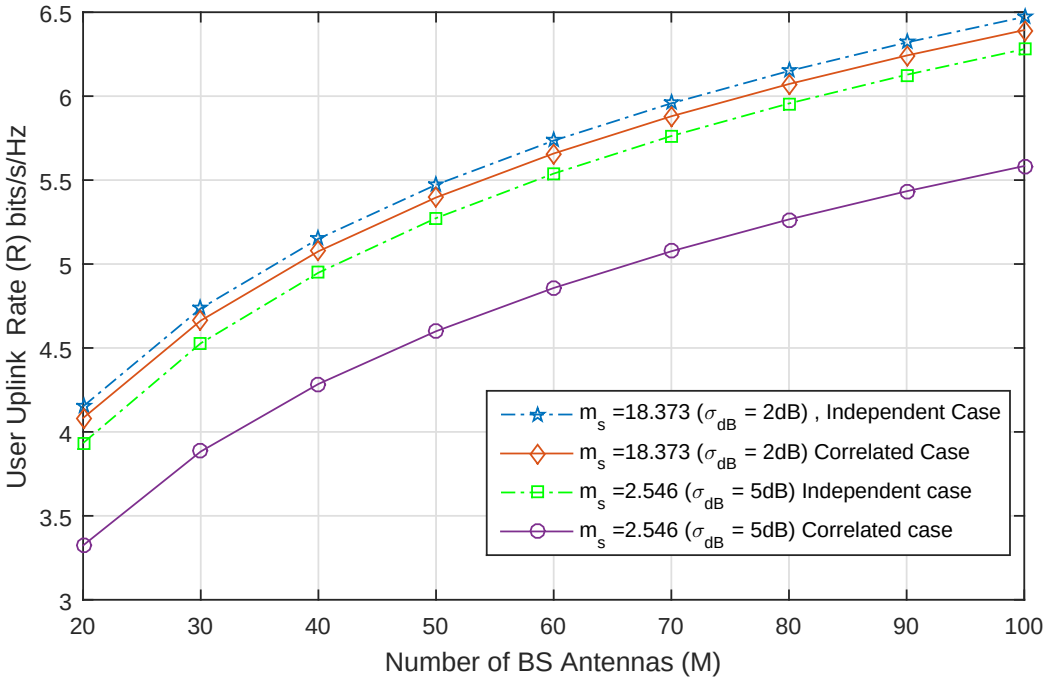

Figure 4.3: Comparison of Ergodic Capacity under Rayleigh Fading with both Independent and fully Correlated Shadowing using MRC receivers ($m_m = 1, \Omega_s = 1$) with transmit power $p_u = 10$ dB.

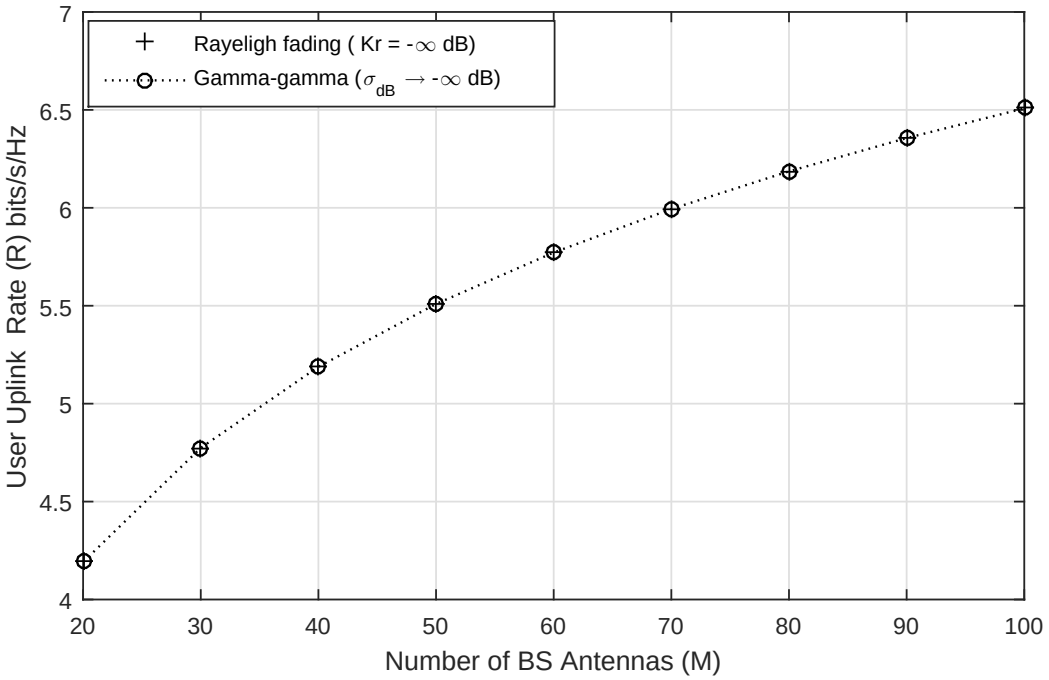

Figure 4.4: Comparison of Ergodic Capacity under Rayleigh Fading and distributed shadowing spread diminished ($m_m = 1, \Omega_s = 1$) with transmit power p_u = 10 dB.

The plot of Figure 4.1 shows the capacity for a desired user under Rayleigh fading (m_m= 1) and independent shadowing at the BS, in comparing this with Figure 3.2 it shows a drop in capacity for the desired user, this is significant because of the presence of shadowing. It can be observed also that as the shadowing spread (σ_{dB}) increases the shadowing parameter (m_s) decreases which indicates severe shadowing conditions and it can be seen from the Figure 4.1 the drop rate in capacity from about 4.3 bits/s/Hz to about 3.2 bits/s/Hz at $M = 20$ antennas, with an increase in σ_{dB} from 2 dB to 9 dB.

In the case of fully correlated shadowing at the BS, as shown in Figure 4.2 the effect of correlation is clearly seen to degrade performance of large-scale MIMO

when antennas are not sufficient spaced with a drop rate of about 3 bits/s/Hz in capacity with an increase in σ_{dB} of about 5 dB, hence the user suffers and the capacity rate drops severely as the shadowing spread increases.

Figure 4.3 shows a comparison for both independent and correlated cases for large-scale fading, it can be seen that for the case of $\sigma_{dB} = 2$ dB the capacity in both cases is similar to each other but as the shadowing spread increases, i.e., when $\sigma_{dB} = 5$ dB, the capacity in the case of correlated shadowing reduces greatly from about 4.2 bits/s/Hz to about 3.3 bits/s/Hz when compared to that for the independent case where the capacity for the desired user reduces from 4.3 bits/s/Hz to about 4 bits/s/Hz with an increase in shadowing spread of 3 dB at $M = 20$ antennas, this shows the effect that correlation has on the capacity in large-scale MIMO systems.

Figure 4.4 shows a comparison when the shadowing spread σ_{dB} tends to zero i.e., no shadowing in the case of independent shadowing with $m_m = 1$ it matches to that of Rayleigh fading where $K_r = 0$ in (Sec 3.2.3) which validates the results and shows without the presence shadowing large-scale MIMO improves capacity of the desired user in the presence of small-scale fading as more antennas are added to the BS.

CHAPTER 5

CONCLUSION

5.1 Conclusions

In this thesis, using moment-based analysis, the ergodic capacity of large-scale MIMO systems was derived. New capacity bounds were developed for large-scale MIMO channels. The bounds developed incorporate both multipath fading and large scale fading (shadowing) for large-scale MIMO systems with an assumption of perfect CSI, where there is a large number of antennas at the BS. Using both MRC and ZF receivers, it was shown that the ZF receivers perform better than MRC in the presence of multipath and interference. It was also shown that as more K single-antennas users are added the capacity increases in magnitude.

This work was split into two major analysis sections, where the large scale fading component was held constant and the multipath fading capacity bounds were derived. Secondly both the shadowing and multipath fading were incorporated as composite fading. Using the tractable gamma-gamma model, new capacity

bounds were derived for this case. The multipath fading was based on Rician fading with Rayleigh and Rician interference, it was shown as the Rician factor K_r increases the uplink sum rate increases, and in the case of shadowing as the shadowing spread (σ_{dB}) increases the shadowing parameter m_s reduces which indicates severe shadowing and results in the reduction of the capacity of the desired user. Both independent and correlated shadowing analysis were carried out and it was shown, using the developed bounds that the capacity of the desired user reduces significantly in the correlated case when compared to independent shadowing.

In summary the main results are:

- Novel expressions for the ergodic capacity bounds for a desired user with Rician multipath fading and independent Rayleigh interferers.
- Novel expressions for the ergodic capacity bounds for a desired user with Rician multipath fading and independent Rician interferers.
- Novel expressions for the ergodic capacity bounds for a desired user with gamma-gamma composite fading with independent shadowing at the BS.
- Novel expressions for the ergodic capacity bounds for a desired user with gamma-gamma composite fading with fully correlated shadowing at the BS.

5.2 Future Research

In this work independent multipath fading was assumed for the development of the capacity bounds with perfect CSI, this can be extended to the case of correlated multipath fading using imperfect CSI. Using the analysis provided telecommunication engineers while building antenna arrays for large-scale MIMO should make sure that there is sufficient spacing between the BS station antennas to avoid correlated shadowing so as to avoid drop in sum rate for desired users.

The analysis provided in this work deals with single-antennas users and this can be extended to multi-antenna systems, where there are multiple users and multi-antennas arrays per user also shadowing with partial correlations, and the case of imperfect CSI can also be considered for future work. In general, large-scale MIMO offers opportunity of increasing capacity at the cost of adding more antennas at the BS and also averages out small-scale fading as more antennas are added but large-scale fading effect still remains.

APPENDIX A

DERIVATIONS OF THE CAPACITY BOUND FOR RICIAN MULTIPATH FADING CHANNELS

In carrying out the analysis an assumption is made for tractability which can be applied to arbitrary number of antennas and interference sources, both $\mathbf{S}_k$ and $\mathbf{S}_i$ are set as column vector of order 2×1. The mean and variance of the new R.V. $\tilde{s}_i$ are derived as follows, from Eqn.(3.18)

$$\mathbb{E}[\tilde{s}_i|\mathbf{s}_k] = \frac{\begin{bmatrix} h_{1,k}^H\sqrt{\gamma_k} & h_{2,k}^H\sqrt{\gamma_k} \end{bmatrix}}{\left\| \begin{bmatrix} h_{1,k}\sqrt{\gamma_k} \\ h_{2,k}\sqrt{\gamma_k} \end{bmatrix} \right\|} \mathbb{E}\left\{ \begin{bmatrix} h_{1,i}\sqrt{\gamma_i} \\ h_{2,i}\sqrt{\gamma_i} \end{bmatrix} \right\}, \tag{A.1}$$

with Rayleigh interferers which are i.i.d, zero-mean unit variance complex Gaussian R.V., therefore $\mathbb{E}\left(h_{1,i}\sqrt{\gamma_i}\right) = \mathbb{E}\left(h_{2,i}\sqrt{\gamma_i}\right) = 0$ therefore Eqn.(A.1) reduces to 0, i.e.,

$$\mathbb{E}[\tilde{s}_i|\mathbf{s}_k] = 0. \tag{A.2}$$

For the variance of $\tilde{s}_i$, Eqn.(3.19) becomes

$$\mathbb{E}\{|\tilde{s}_i|^2\} = \frac{\begin{bmatrix} h_{1,k}^H\sqrt{\gamma_k} & h_{2,k}^H\sqrt{\gamma_k} \end{bmatrix} \mathbb{E}\left[\begin{bmatrix} h_{1,i}\sqrt{\gamma_i} \\ h_{2,i}\sqrt{\gamma_i} \end{bmatrix} \begin{bmatrix} h_{1,i}^H\sqrt{\gamma_i} & h_{2,i}^H\sqrt{\gamma_i} \end{bmatrix} \right] \begin{bmatrix} h_{1,k}\sqrt{\gamma_k} \\ h_{2,k}\sqrt{\gamma_k} \end{bmatrix}}{\left[\begin{bmatrix} h_{1,k}^H\sqrt{\gamma_k} & h_{2,k}^H\sqrt{\gamma_k} \end{bmatrix} \begin{bmatrix} h_{1,k}\sqrt{\gamma_k} \\ h_{2,k}\sqrt{\gamma_k} \end{bmatrix} \right]}. \tag{A.3}$$

Taking the inner term of the numerator in Eqn.(A.3) i.e., $\mathbb{E}[\mathbf{s}_i\mathbf{s}_i^H]$ and evaluating the multiplication of the inner matrices,

$$\mathbb{E}[\mathbf{s}_i\mathbf{s}_i^H] = \mathbb{E}\begin{bmatrix} |h_{1,i}|^2\gamma_i & h_{1,i}h_{2,i}^H\gamma_i \\ h_{1,i}^H h_{2,i}\gamma_i & |h_{2,i}|^2\gamma_i \end{bmatrix}. \tag{A.4}$$

Since the interference coefficients are independent from each other i.e., $(\mathbb{E}[h_{1,i}h_{2,i}^H] = \mathbb{E}[h_{1,i}^H h_{2,i}] = 0)$ then Eqn.(A.4) reduces to

$$\mathbb{E}[\mathbf{s}_i\mathbf{s}_i^H] = \gamma_i \begin{bmatrix} \mathbb{E}\left(|h_{1,i}|^2\right) & 0 \\ 0 & \mathbb{E}\left(|h_{2,i}|^2\right) \end{bmatrix}, \tag{A.5}$$

then

$$\mathbf{s}_k^H\mathbb{E}[\mathbf{s}_i\mathbf{s}_i^H]\mathbf{s}_k = \begin{bmatrix} h_{1,k}^H\sqrt{\gamma_k} & h_{2,k}^H\sqrt{\gamma_k} \end{bmatrix} \gamma_i \begin{bmatrix} \mathbb{E}\left(|h_{1,i}|^2\right) & 0 \\ 0 & \mathbb{E}\left(|h_{2,i}|^2\right) \end{bmatrix} \begin{bmatrix} h_{1,k}\sqrt{\gamma_k} \\ h_{2,k}\sqrt{\gamma_k} \end{bmatrix}. \tag{A.6}$$

Evaluating the terms in Eqn.(A.6) from left to right

$$\begin{aligned} \mathbf{s}_k^H\mathbb{E}[\mathbf{s}_i\mathbf{s}_i^H]\mathbf{s}_k &= \begin{bmatrix} h_{1,k}^H\gamma_i\sqrt{\gamma_k}\{\mathbb{E}\left(|h_{1,i}|^2\right)\} & h_{2,k}^H\gamma_i\sqrt{\gamma_k}\{\mathbb{E}\left(|h_{2,i}|^2\right)\} \end{bmatrix} \begin{bmatrix} h_{1,k}\sqrt{\gamma_k} \\ h_{2,k}\sqrt{\gamma_k} \end{bmatrix} \\ &= \left[|h_{1,k}|^2\gamma_i\gamma_k\{\mathbb{E}\left(|h_{1,i}|^2\right)\} + |h_{2,k}|^2\gamma_i\gamma_k\{\mathbb{E}\left(|h_{2,i}|^2\right)\}\right], \end{aligned} \tag{A.7}$$

by making use of the notation in [28] where $Var(X) = \mathbb{E}[X^2] - (\mathbb{E}[X])^2$, with Rayleigh interferers which are i.i.d, zero-mean, unit variance complex Gaussian

R.V., therefore $\mathbb{E}\left(|h_{1,i}|^2\right) = \mathbb{E}\left(|h_{2,i}|^2\right) = 1$, then Eqn.(A.7) reduces to

$$\mathbf{s}_k^H \mathbb{E}[\mathbf{s}_i \mathbf{s}_i^H] \mathbf{s}_k = \gamma_i \gamma_k \left[|h_{1,k}|^2 + |h_{2,k}|^2\right], \tag{A.8}$$

the denominator in Eqn.(A.3) can be expressed as

$$\begin{aligned} |s_k|^2 = |\mathbf{s}_k^H \mathbf{s}_k| &= \begin{bmatrix} h_{1,k}^H \sqrt{\gamma_k} & h_{2,k}^H \sqrt{\gamma_k} \end{bmatrix} \begin{bmatrix} h_{1,k} \sqrt{\gamma_k} \\ h_{2,k} \sqrt{\gamma_k} \end{bmatrix} \\ &= \gamma_k \left[|h_{1,k}|^2 + |h_{2,k}|^2\right]. \end{aligned} \tag{A.9}$$

Combining the results obtained in Eqn.(A.8) and Eqn.(A.9) in Eqn.(A.3),

$$\begin{aligned} \mathbb{E}\{|\tilde{s}_i|^2\} &= \frac{\gamma_i \gamma_k \left[|h_{1,k}|^2 + |h_{2,k}|^2\right]}{\gamma_k \left[|h_{1,k}|^2 + |h_{2,k}|^2\right]} \\ &= \gamma_i \end{aligned} \tag{A.10}$$

Special Case: No Shadowing i.e., $\gamma_i = 1$ therefore Eqn.(A.10) reduces to

$$\mathbb{E}\{|\tilde{s}_i|^2\} = 1. \tag{A.11}$$

Lemma 1: By setting $\tilde{s}_i \triangleq \frac{\mathbf{s}_k^H \mathbf{s}_i}{\|\mathbf{s}_k\|}$ and conditioning on $\mathbf{s}_k$, and using the results of Eqn.(A.10) in Eqn.(3.20) $\tilde{s}_i$ is a Gaussian R.V. with zero mean and fixed variance γ_i, i.e $\tilde{s}_i \sim \mathcal{CN}\ (0,\gamma_i)$ that independent of $\mathbf{s}_k$.

Therefore achievable rate in Eqn.(3.20) reduces to

$$\tilde{R}_{P,k}^{mrc} = \left(p_u \sum_{i=1, i \neq k}^{K} \gamma_i + 1\right) \mathbb{E}\left\{\frac{1}{p_u \parallel \mathbf{s}_k \parallel^2}\right\} \tag{A.12}$$

The second term in Eqn.(A.12) $\parallel \mathbf{s}_k \parallel^2$ follows a noncentral chi-squared distribution ($\chi^2_{p,\xi}$) with $p = 2M$ degrees of freedom and centrality parameter $\xi = 2K_rM$, where K_r is the Rice factor (See Sec. 2.3.3) [53]. It follows then that the **Exact** n-th inverse moment of the noncentral chi-squared distribution is given by [64][65],

$$\mathbb{E}\left\{\left(\frac{1}{\chi^2_{p,\xi}}\right)^n\right\} = \quad {}_1F_1\left(\frac{p}{2}-n, \frac{p}{2}; \frac{\xi}{2}\right)\frac{e^{-\frac{\xi}{2}}}{2^n}\frac{\Gamma(\frac{p}{2}-n)}{\Gamma(\frac{p}{2})} \ , \tag{A.13}$$

where ${}_1F_1\left(\frac{p}{2}-n, \frac{p}{2}; \frac{\xi}{2}\right)$ is the Krummer confluent hypergeometric function.

By setting $n = 1$, $p = 2M$ and $\xi = 2K_rM$ we have, Eqn.(A.13) becomes

$$\mathbb{E}\left\{\left(\frac{1}{\chi^2_{p,\xi}}\right)\right\} = \quad {}_1F_1\left(M-1, M; K_rM\right)\frac{e^{-K_rM}}{2}\frac{\Gamma(M-1)}{\Gamma(M)} \ , \tag{A.14}$$

and $\Gamma(\cdot)$ is the gamma function [66].

Since $\dfrac{\Gamma(M-1)}{\Gamma(M)} = \dfrac{1}{M-1}$ and replacing this in Eqn.(A.14)

$$\mathbb{E}\left\{\left(\frac{1}{\chi^2_{p,\xi}}\right)\right\} = \quad {}_1F_1\left(M-1, M; K_rM\right)\frac{e^{-K_rM}}{2}\frac{1}{M-1} \ . \tag{A.15}$$

Using Eqn.(A.15) therefore a closed expression for the second term in Eqn.(A.12) is derived as,

$$\mathbb{E}\left\{\frac{1}{p_u \parallel \mathbf{s}_k \parallel^2}\right\} = \quad {}_1F_1\left(M-1, M; K_rM\right)\frac{e^{-K_rM}}{2}\frac{1}{(M-1)p_u} \ , \tag{A.16}$$

Instead of using Eqn.(A.13) the asymptotic expression for the n-th inverse moment of the noncentral chi-squared distribution can also be used in the following lemma.

Lemma 2: The **Asymptotic** expansion of the n-th inverse moment of the noncentral chi-squared distribution is stated from [64] as,

$$\mathbb{E}\left\{\left(\frac{1}{\chi^2_{p,\xi}}\right)^n\right\} = \quad A_1\left(p,\frac{\xi}{n}\right) + A_2\left(p,\frac{\xi}{n}\right) + A_3\left(p,\frac{\xi}{n}\right) + O\left(p^{-n-3}\right) \quad , \quad \text{(A.17)}$$

where

$$A_1\left(p,\tfrac{\xi}{n}\right) = \frac{1}{(p+\xi)^n} \ ,$$
$$A_2\left(p,\tfrac{\xi}{n}\right) = \frac{n(n+1)(p+2\xi)}{(p+\xi)^{n+2}},$$
$$A_3\left(p,\tfrac{\xi}{n}\right) = \frac{n(n+1)(n+2)\{(3n+1)p^2+(12n+4)p\xi+(12n+12)\xi^2\}}{6(p+\xi)^{n+4}}$$

by making use of the first and second term only in Eqn.(A.17) and inputing the values for n, p and ξ ,

$$A_1\left(p,\xi\right) = \frac{1}{2M(1+K_r)} \ ,$$
$$A_2\left(p,\xi\right) = \frac{(2)(2M+4K_rM)}{(2M+2K_rM)^3} = \frac{4(M+2K_rM)}{(2M+2K_rM)^3}.$$

Using the above values for the first and second term in Eqn.(A.17),

$$\begin{aligned}\mathbb{E}\left\{\left(\tfrac{1}{\chi^2_{p,\xi}}\right)\right\} &= \frac{1}{2M(1+K_r)} + \frac{4(M+2K_rM)}{(2M+2K_rM)^3} \\ &= \frac{8M(1+K_r)(M+2K_rM)+(2M+2K_rM)^3}{2M(1+K_r)(2M+2K_rM)^3} \ ,\end{aligned} \quad \text{(A.18)}$$

therefore using Eqn.(A.18) the second term in Eqn.(A.12) can be written as

$$\mathbb{E}\left\{\frac{1}{p_u \parallel \mathbf{s}_k \parallel^2}\right\} = \frac{8M(1+K_r)(M+2K_rM)+(2M+2K_rM)^3}{2Mp_u(1+K_r)(2M+2K_rM)^3} \ . \tag{A.19}$$

Based on Eqn.(A.16), two important properties of the Krummer confluent hypergeometric function occurs when the last term K_rM either goes to zero (K_r= 0) or grows large ($M \to \infty$) [66][67].

When *a,b* is fixed and $|z| = 0$

$$ {}_1F_1\left(a,b;z\right) = 1 \ , \tag{A.20}$$

and using [68] *a,b* is fixed and $|z| \to \infty$

$$ {}_1F_1\left(a,b;z\right) = \frac{\Gamma(b)(-z)^{-a}}{\Gamma(b-a)}\left[\sum_{k=0}^{n}\frac{(-1)^k(a)_k(a-b+1)_k \ z^k}{k!}+O(z^{-n-1})\right] + \frac{e^z z^{a-b}\Gamma(b)}{\Gamma(a)}\left[\sum_{k=0}^{n}\frac{(b-a)_k(1-a)_k \ z^k}{k!}+O(z^{-n-1})\right] \ , \tag{A.21}$$

where $(a)_k$ is called the **Pochhamer** symbol [68].

By substituting Eqn.(A.16) in Eqn.(A.12) we obtain

$$\mathbb{E}\left\{\frac{p_u\sum\limits_{i=1,i\neq k}^{K}|\tilde{s}_i|^2+1}{p_u \parallel \mathbf{s}_k \parallel^2}\right\} = \left(p_u\sum_{i=1,i\neq k}^{K}\gamma_i+1\right)\left({}_1F_1\left(M-1,M;K_rM\right)\frac{e^{-K_rM}}{2}\frac{1}{(M-1)p_u}\right) \ . \tag{A.22}$$

APPENDIX B

DERIVATION FOR THE INVERSE MOMENT OF GAMMA-GAMMA DISTRIBUTION.

The next step is to derive the inverse moment of the gamma-gamma distribution to be used in Eqn.(3.20) i.e. $\mathbb{E}\left\{\frac{1}{\parallel \mathbf{s}_{km} \parallel^2}\right\}$. By rewriting Eqn.(4.6) in a compact manner [69],

$$f_s(s) = \frac{2\Xi^{\frac{\beta+1}{2}} s^{\frac{\beta-1}{2}}}{\Gamma(\tilde{m}_s)\Gamma(\tilde{m}_m)} K_\alpha \left[2s^{1/2}\sqrt{\Xi}\right], \qquad s \geq 0 \tag{B.1}$$

where $\alpha = \tilde{m}_s$ - $\tilde{m}_m$, $\beta = \tilde{m}_s + \tilde{m}_m$ -1 and $\Xi = \tilde{m}_s\tilde{m}_m/\tilde{\Omega}$.

Using [70] the inverse moment of the gamma-gamma model using the its PDF is derived,

$$\begin{aligned} \mathbb{E}\left[\tfrac{1}{s}\right] &= \int_0^\infty \frac{f_s(s)}{s} ds \\ &= \frac{2\Xi^{\frac{\beta+1}{2}}}{\Gamma(\tilde{m}_s)\Gamma(\tilde{m}_m)} \int_0^\infty s^{\frac{\beta-3}{2}} K_\alpha \left[2s^{1/2}\sqrt{\Xi}\right] ds \end{aligned} \tag{B.2}$$

applying a change of variable in Eqn.(B.2) i.e., let $x = s^{1/2}$ therefore $2x\mathrm{dx} = \mathrm{ds}$, rearranging the indices and substituting this in the above equation, Eqn.(B.2) reduces to

$$\mathbb{E}\left[\frac{1}{s}\right] = \frac{4\Xi^{\frac{\beta+1}{2}}}{\Gamma(\tilde{m}_s)\Gamma(\tilde{m}_m)} \int_0^\infty x^{\beta-2} K_\alpha \left[2x\sqrt{\Xi}\right] dx \tag{B.3}$$

The integral in Eqn.(B.3) is evaluated using [29, eq.(6.561/16)] i.e.,

$$\int_0^\infty x^\mu K_v(ax)\, dx = 2^{\mu-1} a^{-\mu-1} \Gamma\left(\frac{1+\mu+v}{2}\right) \Gamma\left(\frac{1+\mu-v}{2}\right), \tag{B.4}$$

by setting $\mu = \beta$-2, $a = 2\sqrt{\Xi}$ and $v = \alpha$, and replacing the original values of β and α in Eqn.(B.2), the inverse moment of the gamma- gamma distribution can

be expressed as

$$\mathbb{E}\left[\frac{1}{s}\right] = \frac{\Gamma(\tilde{m}_s - 1)\Gamma(\tilde{m}_m - 1)\Xi}{\Gamma(\tilde{m}_s)\Gamma(\tilde{m}_m)}. \tag{B.5}$$

REFERENCES

[1] C. Oestges and B. Clerckx, *MIMO wireless communications: from real-world propagation to space-time code design.* Academic Press, 2010.

[2] Q. H. Spencer, C. B. Peel, A. L. Swindlehurst, and M. Haardt, "An introduction to the Multi-User MIMO downlink," *IEEE Communications Magazine*, vol. 42, no. 10, pp. 60–67, 2004.

[3] D. Gesbert, M. Kountouris, R. W. Heath, C.-B. Chae, and T. Salzer, "Shifting the MIMO paradigm," *IEEE Signal Processing Magazine*, 2007.

[4] T. Kailath and A. J. Paulraj, "Increasing capacity in wireless broadcast systems using distributed transmission/directional reception," Sep. 6 1994, uS Patent 5,345,599.

[5] T. M. Duman and A. Ghrayeb, *Front Matter.* Wiley Online Library, 2007.

[6] A. Sibille, C. Oestges, and A. Zanella, *MIMO: from theory to implementation.* Academic Press, 2010.

[7] A. Chockalingam and B. S. Rajan, *Large MIMO Systems.* Cambridge University Press, 2014.

[8] T. L. Marzetta, G. Caire, M. Debbah, I. Chih-Lin, and S. K. Mohammed, "Special issue on massive MIMO," *Journal of Communications and Networks*, vol. 15, no. 4, pp. 333–337, 2013.

[9] J. G. Andrews, S. Buzzi, W. Choi, S. Hanly, A. Lozano, A. C. Soong, and J. C. Zhang, "What will 5G be?" 2014.

[10] N. Instruments and L. University. (2014) National instruments. [Online]. Available: http://www.ni.com/white-paper/52382/en/

[11] T. L. Marzetta, "Noncooperative cellular wireless with unlimited numbers of base station antennas," *IEEE Transactions on Wireless Communications*, vol. 9, no. 11, pp. 3590–3600, 2010.

[12] H. Q. Ngo, E. G. Larsson, and T. L. Marzetta, "Energy and spectral efficiency of very large multiuser MIMO systems," *IEEE Transactions on Communications*, vol. 61, no. 4, pp. 1436–1449, 2013.

[13] F. Rusek, D. Persson, B. K. Lau, E. G. Larsson, T. L. Marzetta, O. Edfors, and F. Tufvesson, "Scaling up MIMO: Opportunities and challenges with very large arrays," *IEEE Signal Processing Magazine*, vol. 30, no. 1, pp. 40–60, 2013.

[14] A. Goldsmith, S. A. Jafar, N. Jindal, and S. Vishwanath, "Capacity limits of MIMO channels," *IEEE Journal on Selected Areas in Communications*, vol. 21, no. 5, pp. 684–702, 2003.

[15] B. Clerckx and C. Oestges, *MIMO Wireless Networks: Channels, Techniques and Standards for Multi-antenna, Multi-user and Multi-cell Systems*. Academic Press, 2013.

[16] H. K. Bizaki, "MIMO systems, theory and applications," *InTech, Rijeka*, 2011.

[17] T. Brown, P. Kyritsi, and E. De Carvalho, *Practical Guide to MIMO Radio Channel: with MATLAB Examples*. John Wiley & Sons, 2012.

[18] M. Salehi and J. Proakis, "Digital communications," *McGraw–Hill, New York*, 2008.

[19] E. M. I. Observatory. (2011) Executive summary. [Online]. Available: http://www.gsma.com/publicpolicy/wp-content/uploads/2012/04/emoeswebfinal.pdf

[20] F. Haider, X. Gao, X.-H. You, Y. Yang, D. Yuan, H. M. Aggoune, and H. Haas, "Cellular architecture and key technologies for 5G wireless communication networks," *IEEE Communications Magazine*, p. 123, 2014.

[21] V. Jungnickel, K. Manolakis, W. Zirwas, B. Panzner, V. Braun, M. Lossow, M. Sternad, T. Svensson *et al.*, "The role of small cells, coordinated multipoint, and massive MIMO in 5G," *IEEE Communications Magazine*, vol. 52, no. 5, pp. 44–51, 2014.

[22] P. Demestichas, A. Georgakopoulos, D. Karvounas, K. Tsagkaris, V. Stavroulaki, J. Lu, C. Xiong, and J. Yao, "5G on the horizon: key chal-

lenges for the radio-access network," , *IEEE Vehicular Technology Magazine*, vol. 8, no. 3, pp. 47–53, 2013.

[23] A. Goldsmith, *Wireless communications*. Cambridge university press, 2005.

[24] D.-S. Shiu, G. J. Foschini, M. J. Gans, and J. M. Kahn, "Fading correlation and its effect on the capacity of multielement antenna systems," *IEEE Transactions on Communications*, vol. 48, no. 3, pp. 502–513, 2000.

[25] T. S. Rappaport *et al.*, *Wireless communications: principles and practice*, 2002, vol. 2.

[26] D. Tse and P. Viswanath, *Fundamentals of wireless communication*. Cambridge university press, 2005.

[27] E. Telatar, "Capacity of multi-antenna gaussian channels," *European transactions on telecommunications*, vol. 10, no. 6, pp. 585–595, 1999.

[28] A. Papoulis and S. U. Pillai, *Probability, random variables, and stochastic processes*. Tata McGraw-Hill Education, 2002.

[29] I. S. Gradshtejn and I. M. Ryzhik, *Table of integrals, series and products*. Academic Press, 1965.

[30] I. Kostić, "Analytical approach to performance analysis for channel subject to shadowing and fading," *IEE Proceedings-Communications*, vol. 152, no. 6, pp. 821–827, 2005.

[31] S. Al-Ahmadi and H. Yanikomeroglu, "On the statistics of the sum of correlated generalized-K rvs," in *2010 IEEE International Conference on Communications (ICC)*. IEEE, 2010, pp. 1–5.

[32] L. Lu, G. Li, A. Swindlehurst, A. Ashikhmin, and R. Zhang, "An Overview of Massive MIMO: Benefits and challenges," *IEEE Signal Processing Magazine*, 2013.

[33] U. of Toronto. (2014) Recieve diversity. [Online]. Available: http://www.comm.utoronto.ca/ rsadve/Notes/DiversityReceive.pdf

[34] Y.-W. P. Hong, W.-J. Huang, and C.-C. J. Kuo, *Cooperative communications and networking: technologies and system design*. Springer Science & Business Media, 2010.

[35] H. Q. Ngo, E. G. Larsson, and T. L. Marzetta, "Massive MU-MIMO downlink tdd systems with linear precoding and downlink pilots," *arXiv preprint arXiv:1310.1510*, 2013.

[36] E. G. Larsson, O. Edfors, F. Tufvesson, and T. L. Marzetta, "Massive MIMO for next generation wireless systems," *arXiv preprint arXiv:1304.6690*, 2013.

[37] Y. Yifei and Z. Longming, "Application scenarios and enabling technologies of 5G," *Communications, China*, vol. 11, no. 11, pp. 69–79, 2014.

[38] P. K. Agyapong, M. Iwamura, D. Staehle, W. Kiess, and A. Benjebbour, "Design considerations for a 5G network architecture," *IEEE Communications Magazine*, vol. 52, no. 11, pp. 65–75, 2014.

[39] J. Zhang, C.-K. Wen, S. Jin, X. Gao, and K.-K. Wong, "On capacity of large-scale MIMO multiple access channels with distributed sets of correlated antennas," *arXiv preprint arXiv:1209.5513*, 2012.

[40] H. Wu, L. Wang, X. Wang, and X. You, "Asymptotic and non-asymptotic analysis of uplink sum rate for relay-assisted MIMO cellular systems," *IEEE Transactions on Signal Processing*, 2014.

[41] M. Matthaiou, N. D. Chatzidiamantis, G. K. Karagiannidis, and J. A. Nossek, "On the capacity of generalized-fading MIMO channels," *IEEE Transactions on Signal Processing*, vol. 58, no. 11, pp. 5939–5944, 2010.

[42] W. Weichselberger, M. Herdin, H. Ozcelik, and E. Bonek, "A stochastic MIMO channel model with joint correlation of both link ends," *IEEE Transactions on Wireless Communications*, vol. 5, no. 1, pp. 90–100, 2006.

[43] S. Chatzinotas and B. Ottersten, "Coordinated multipoint uplink capacity over a MIMO composite fading channel," in *2012 International Conference on Computing, Networking and Communications (ICNC)*. IEEE, 2012, pp. 1061–1065.

[44] E. Bjornson, J. Hoydis, M. Kountouris, and M. Debbah, "Massive MIMO systems with non-ideal hardware: Energy efficiency, estimation, and capacity limits," *arXiv preprint arXiv:1307.2584*, 2013.

[45] J. Hoydis, S. Ten Brink, M. Debbah *et al.*, "Massive MIMO in the ul/dl of cellular networks: How many antennas do we need?" *IEEE Journal on selected Areas in Communications*, vol. 31, no. 2, pp. 160–171, 2013.

[46] Q. Zhang, S. Jin, K.-K. Wong, H. Zhu, and M. Matthaiou, "Power scaling of uplink Massive MIMO systems with arbitrary-rank channel means," *IEEE Transactions on Communications*, 2014.

[47] E. P. Tsakalaki, O. N. Alrabadi, E. De Carvalho, and G. F. Pedersen, "On the beamforming performance of large-scale antenna arrays," in *Antennas and Propagation Conference (LAPC), 2012 Loughborough*. IEEE, 2012, pp. 1–4.

[48] U. Madhow, D. R. Brown, S. Dasgupta, and R. Mudumbai, "Distributed massive MIMO: algorithms, architectures and concept systems," in *Information Theory and Applications Workshop (ITA), 2014*. IEEE, 2014, pp. 1–7.

[49] H. Li and V. Leung, "Low complexity zero-forcing beamforming for distributed massive MIMO systems in large public venues," *Journal of Communications and Networks*, vol. 15, no. 4, pp. 370–382, 2013.

[50] J. Choi, Z. Chance, D. Love, and U. Madhow, "Noncoherent trellis coded quantization: A practical limited feedback technique for massive MIMO systems," 2013.

[51] J. Sung and W. Sung, "Large-scale MIMO beamforming using successive channel state estimation and codebook extension," in *IEEE 24th International Symposium on Personal Indoor and Mobile Radio Communications (PIMRC)*. IEEE, 2013, pp. 408–413.

[52] S. Jin, X. Wang, Z. Li, and K.-K. Wong, "Zero-forcing beamforming in massive MIMO systems with time-shifted pilots," in *IEEE International Conference on Communications (ICC)*. IEEE, 2014, pp. 4801–4806.

[53] A. Shah and A. M. Haimovich, "Performance analysis of maximal ratio combining and comparison with optimum combining for mobile radio communications with cochannel interference," *IEEE Transactions on Vehicular Technology*, vol. 49, no. 4, pp. 1454–1463, 2000.

[54] R. J. Muirhead, *Aspects of multivariate statistical theory*. John Wiley & Sons, 2009, vol. 197.

[55] A. K. Gupta and D. K. Nagar, *Matrix variate distributions*. CRC Press, 1999, vol. 104.

[56] A. Ullah, "On the inverse moments of non-central wishart matrix," The A. Gary Anderson Graduate School of Management. University of California Riverside, Tech. Rep., 1990.

[57] D. L. of Mathematical Functions. (2014) Function of matrix argument. [Online]. Available: http://dlmf.nist.gov/35.3

[58] C. Wang, E. K. Au, R. D. Murch, W. H. Mow, R. S. Cheng, and V. Lau, "On the performance of the MIMO zero-forcing receiver in the presence of channel estimation error," *IEEE Transactions on Wireless Communications*, vol. 6, no. 3, pp. 805–810, 2007.

[59] S. Al-Ahmadi and H. Yanikomeroglu, "On the approximation of the generalized-K distribution by a gamma distribution for modeling composite fading channels," *IEEE Transactions on Wireless Communications*, vol. 9, no. 2, pp. 706–713, 2010.

[60] S. Al-Ahmadi, "The gamma-gamma signal fading model: A survey [wireless corner]," *IEEE Antennas and Propagation Magazine*, vol. 56, no. 5, pp. 245–260, 2014.

[61] G. K. Karagiannidis, T. A. Tsiftsis, and R. K. Mallik, "Bounds for multihop relayed communications in nakagami-m fading," *IEEE Transactions on Communications*, vol. 54, no. 1, pp. 18–22, 2006.

[62] N. D. Chatzidiamantis and G. K. Karagiannidis, "On the distribution of the sum of gamma-gamma variates and applications in RF and optical wireless communications," *IEEE Transactions on Communications*, vol. 59, no. 5, pp. 1298–1308, 2011.

[63] E. statistics handbook. (2014) Lognormal distribution. [Online]. Available: http://www.itl.nist.gov/div898/handbook/eda/section3/eda3669.htm

[64] T. Fujioka, "Asymptotic approximations of the inverse moment of the non-central chi-squared variable," *Journal of the Japan Statistical Society*, vol. 31, no. 1, pp. 99–109, 2001.

[65] M. Bock, G. G. Judge, and T. Yancey, "A simple form for the inverse moments of non-central chi squared random variables and certain confluent hypergeometric functions," *Journal of Econometrics*, vol. 25, no. 1, pp. 217–234, 1984.

[66] N. N. Lebedev, *Special functions and their applications*. Courier Dover Publications, 1972.

[67] N. L. Johnson and S. Kotz, *Distributions in Statistics: Continuous Univariate Distributions: Vol.: 2*. Houghton Mifflin, 1970.

[68] W. R. Inc. (2007) Hypergeometric functions. [Online]. Available: http://functions.wolfram.com/HypergeometricFunctions/Hypergeometric1F1/06/02/0004/

[69] P. S. Bithas, N. C. Sagias, P. T. Mathiopoulos, G. K. Karagiannidis, and A. A. Rontogiannis, "On the performance analysis of digital communications over generalized-K fading channels," *IEEE Communications Letters*, vol. 10, no. 5, pp. 353–355, 2006.

[70] A. Lozano, A. M. Tulino, and S. Verdú, "Multiple-antenna capacity in the low-power regime," *IEEE Transactions on Information Theory*, vol. 49, no. 10, pp. 2527–2544, 2003.

DARAMOLA, Toluwani Oluwatobi

Building 801 Apt 106, King Fahd University of Petroleum Residential Apartments,Saudi Arabia
Mobile: +966-55-175-8167 Email: toluwanidaramola@yahoo.com

CAREER SUMMARY

An experienced Computer/Communications Engineer who loves being part of a productive team. Quick to embrace new ideas and develop intuitive solutions to problems. Excellent working knowledge of workstations, computers, peripheral devices, networking and telecommunication equipments. I also possess an exceptional ability to communicate efficiently across all management levels. Some of my key areas are:

- Service Management
- Network Planning
- Network Infrastructure
- Performance Optimization
- MIMO Systems
- VSAT Networks
- Business Operations
- Management Consulting

EDUCATION

Master of Science, Telecommunications Engineering
King Fahd University of Petroleum and Minerals,Saudi Arabia (GPA 3.57/4.0) *May 2015.*

Bachelor of Science, Electronics and Computer Engineering (Hons)
Lagos State University, Ojo, Nigeria. (GPA 4.41/5.0) *March 2010.*

PROFESSIONAL EXPERIENCE

Department of Electrical Engineering, KFUPM - Research Assistant *Sept, 2013-present.*

- Participated in various research projects on Distributed Antennas and MIMO Systems.
- Facilitating undergraduate classes by conducting lab session, grading homework and proctoring examinations
- Provided IT support for students and staff of the Nigerian Community in KFUPM.

DHL SUPPLY CHAIN, Alausa-Ikeja, Lagos, Nigeria. *2012- 2013.*
Information Technology Dept. (ISM Team Member)

- Provided IT Support for Users, Peripheral devices and Computer Servers.
- Scheduled and implemented both corrective and preventive maintenance duties to prevent any network downtime.
- Preparation of workstations and servers for users.
- Applications support - backups, upgrades, patches upload,e.t.c.
- Implemented standard processes and support models in line with group directives(global core build, file services, etc).

Yorix Technologies Limited, Berger, Lagos, Nigeria. *2011 - 2012.*
Information Technology and Communication Unit. (Network Engineer)

- Provided IT support and LAN configuration.
- Planned and Executed Wireless Network Projects.
- Troubleshooted and repaired faulty computers.

Information Connectivity Solutions Limited, VI, Lagos, Nigeria. *2009 - 2011.*
Transmission Unit (Wireless & Satellite Comm. Engineer)

- Planned, designed and implemented Radio Frequency networks.
- Installed and maintained Wireless Access Points and Base Stations.
- Deployed Metropolitan Wireless links for ABC project in Lagos State.
- Turned-up and commissioned newly installed transmission links.
- Installed VSAT equipment for both Data and Internet Services for clients.
- Provided Technical support for both Wireless and Satellite clients.

Helbon Associates Limited, Lagos. Nigeria *2008.*
Information Technology Dept. (IT support Engineer)
Workstation installations for clients.
Responsible for managing computer peripherals.
General IT support for company.

AWARDS

KFUPM Graduate Fellowship *2013-2015.*
AECES Award for Excellence Best Male Student *2006, 2007, 2009.*
Lagos State University Scholarship Merit Award *2006-2008.*
Lagos State Government Undergraduate Scholarship *2005-2009.*

CERTIFICATIONS & MEMBERSHIPS

- Microsoft Certified Solutions Associate (MCSA) in View
- TCO Certified Telecommunications Network Specialist (CTNS).
- GVF Certification on Core Skills for VSAT Installers.
- Diploma in Desktop publishing and Microsoft office Suite.
- Institute of Electrical and Electronics Engineers(IEEE).
- Nigerian Society of Engineers(NSE).
- Telecommunications Certification Organization(TCO).
- International Association of Engineers (IAENG)
- Teracom Training Institute
- Global VSAT Forum. (GVF)

SOFTWARE PACKAGES

- Research experience in MATLAB, Simulink, C programming, Maple, .
- Ekahau-Wifi Design Tool,Pathloss, MapInfo .
- Good knowledge of Linux environment.
- Good knowledge of LaTeX for research purposes.
- Windows: (8.1,8, 7, Vista, XP) and Microsoft Office suites: (Word, Excel ,PowerPoint, Project)

SKILLS

- Proficient in VSAT Technologies, Equipments and Installations.
- Installation and configuring of wireless routers and access points.
- Ability to assemble, install and troubleshoot a wide array of computer systems, workstations,servers and peripheral hardware.
- Installation and Handling of communication devices, routers, microwave radios .etc.
- Ability to perform hardware and software installations and provide high-level customer care, and technical support.
- Strong technical knowledge of wired and wireless networks.
- Able to communicate complex IT issues to suppliers and non-technical staff.
- Ability to work well in a team environment
- IT security experience including anti-virus / malware, encryption deployment. Experience of web content management systems

PUBLICATIONS

- T. Daramola, S. Alahamadi,"Ergodic Capacity of large-scale MIMO systems under Rician multipath fading channels", submitted to IEEE Communication letters, May 2015.
- T. Daramola, S. Alahamadi, "Ergodic Capacity of large-scale MIMO systems in shadowed fading channels", submitted to IEEE Communication letters, May 2015.

PROFESSIONAL REFERENCES

- Available on Request.